Thesis for The Degree of Licentiate of Engineering

Transient Spray Mode Fuel Injection

Lokesh Mopuri

Energy Conversion and Propulsion Systems
Department of Mechanics and Maritime Sciences
Chalmers University of Technology
Gothenburg, Sweden, 2023

Transient Spray Mode Fuel Injection

Lokesh Mopuri

Thesis for The Degree of Licentiate of Engineering
Energy Conversion and Propulsion Systems
Department of Mechanics and Maritime Sciences
Chalmers University of Technology
SE-412 96 Göteborg,
Sweden
Phone: +46(0)31 772 1000

Printed by Chalmers Digitaltryck,
Göteborg, Sweden 2023.

To My Advisors and Beloved Family

Abstract

This research examines the pivotal role of transient fuel spray in internal combustion engines, primarily focusing on their influence on dual-fuel (DF) engines. In the case of dual-fuel (DF) engines functioning in a gas mode, the controlling of the primary fuel's ignition is usually managed through the direct injection of liquid pilot fuel. The initial penetration and overall quantity of liquid pilot fuel play a significant role in influencing both the emissions released in the exhaust and the stability of combustion. Different methodologies are employed here to comprehensively explore spray characteristics from multi-hole diesel fuel injectors within a constant-volume spray chamber. The first methodology involves using a nozzle equipped with a thimble structure to isolate a single plume. In contrast, the second approach, known as plume-blocking, entails sealing the orifices of the multi-hole nozzle to generate a single spray plume. Comparisons between these methods reveal that plume-blocking achieves superior spray penetration, although with potential limitations in its applicability to single-spray studies. Furthermore, the research highlights that a clogged nozzle displays distinct spray characteristics compared to an multi-hole (MH) nozzle, whereas a thimble-equipped nozzle yields similar outcomes to the standard MH nozzle. The blocking of orifices within the nozzle modifies the flow distribution within the sac volume, thereby influencing spray characteristics. Another aspect of this study addresses concerns arising from inconsistent performance attributed to manufacturing variations in diesel injectors. The research carefully examines sprays from four different injectors. Experimental studies are conducted under diverse injection conditions, including varying ambient gas densities, injection pressures. Root Mean Square Error (RMSE) analysis is employed to investigate variations in spray penetration length among the injectors, providing details on both symmetric and asymmetric spray behaviours. Furthermore, the study investigates into the behaviour of transient single spray, utilizing a thimble approach, under high-pressure and high-temperature conditions. To maintain an inert and reactive atmosphere, pre-combustion of a lean hydrogen-air mixture is thoroughly achieved. The evaporating and non-reacting spray investigation takes place with the gas composition inside the chamber maintained at approximately 0% oxygen. Spray vapour phases are captured using shadowgraph and Schlieren imaging techniques. Additionally, the study explores the reactive spray with increasing oxygen levels above 0%, employing natural luminosity and Schlieren imaging. The conditions include a temperature range between 400 and 1000 K and fuel injection pressures ranging from 1700 to 2100 bar, resulting in simulated mixture densities ranging from approximately 14.62 to 27.69 kg/m^3. The study emphasizes the considerable effects that temperature, density, and injection pressure have on the characteristics of these sprays.

Keywords

Spray characteristics, thimble structure, clogged nozzle, non-evaporative and reactive spray

List of Publications

Appended publications

This thesis is based on the following publications:

[**Paper I**] **Lokesh Mopuri, Viljam Grahn, David Sedarsky and Jari Hyvönen**, *Shape/penetration analysis of isolated spray plumes in a multi-hole Diesel spray*
Submitted to Experiments in Fluids, under review.

[**Paper II**] **Lokesh Mopuri, Viljam Grahn, David Sedarsky and Jari Hyvönen**, *Manufacturing disparities and their effect on transient spray characteristics in Diesel injectors*
Submitted to Fuel, under review.

Acknowledgment

First and foremost, I would like to express my profound gratitude to my thesis supervisor, Prof. David Sedarsky. His expertise, understanding, generous guidance, and dedication of precious time and unwavering support have allowed me to immerse myself deeply into a topic that has greatly captivated my interest. His mentorship has been a strong source of motivation throughout my research journey. I am deeply thankful for his consistent assistance, insightful suggestions, and encouraging words. I would also like to sincerely thank my co-supervisor sincerely, Dr. Jari Hyvönen from Wärtsilä, for providing unwavering encouragement at various stages of this project. Additionally, my gratitude extends to Wärtsilä for generously providing the necessary platform on their premises to conduct this research, which undeniably made significant contributions to its success. Acknowledgement is also extended to Prof. Mats Andersson for his valuable suggestions and feedback provided at various stages of my research work. Furthermore, my gratitude extends to Viljam Grahn for his invaluable assistance in conducting experiments and engaging in enlightening discussions. His support has played a crucial role in various stages of completing this work, and my time in Vaasa, Finland, particularly during outdoor winter activities, has been truly delightful. Special thanks are due to the professors, research engineers, and labmates at ECaPS, Chalmers, and Wärtsilä for their continuous assistance and guidance, which have been invaluable throughout this journey. I extend my heartfelt appreciation to Dr. Senthil Kumar Parimalanathan, a researcher and my dearest friend at Interfaces and Processes (TIPs) Laboratory, ULB, whose motivation and insightful conversations have constantly encouraged me. He has generously dedicated his valuable time to clarify my doubts and engage in meaningful discussions. Last but certainly not least, I want to express my deepest gratitude to my family for their unwavering support and encouragement. Their steadfast belief in my pursuits has been a constant source of motivation and strength.

Contents

Part I

Introductory chapters

Chapter 1

Introduction

1.1 Background

Conventional diesel engines are highly valued for their compatibility, efficiency, dependability, and cost-effectiveness, and energy density. However, they emit oxides of nitrogen (NO_x) and particulate matter (PM), which are detrimental to human life and the environment [1]. Alternative fuels are being recognized as a potential solution to reduce greenhouse gas emissions and address the challenge of balancing energy demands with dwindling oil reserves [2]. In this context, natural gas is gaining attention as a promising and viable alternative energy source for conventional diesel engines [3], which is also affordable and available worldwide [4]. Today, natural gas is widely regarded as a viable transition fuel, bridging the gap until fully carbon-free and green e-fuels become readily available. Natural gas is a crucial fuel source predominantly extracted from onshore and offshore dedicated gas fields. During extraction, it often contains water and CO_2 which are subsequently separated. The gas is then refined to isolate lighter hydrocarbons from the heavier ones, such as methane and ethane. This lighter fraction can be compressed into Compressed Natural Gas (CNG) or liquefied into Liquefied Natural Gas (LNG) for various uses [5]. While some natural gas also emerges alongside oil extraction, the dedicated natural gas fields remain the primary source. In dual-fuel (DF) compression ignition (CI) engines, natural gas exhibits poor ignition characteristics due to its lower cetane number and auto-ignition temperature compared to diesel fuel [6]. Therefore, an ignition source is always necessary to ignite the natural gas in the cylinder. During the intake stroke, gas is introduced into the cylinder, and a small amount of high-cetane fuel (Diesel) is used to ignite the lean air-gas mixture. To achieve low NO_x emissions, injected fuel must be minimal. Typically, injecting less than 10% diesel fuel at nominal load results in NO_x emissions approximately one-tenth of a standard diesel engine [7]. Moreover, to avoid knocking and misfiring while operating DF engines in gas mode, the timing and quantity of micro-pilot injection must be precisely controlled to keep each cylinder at its optimal operating point [8].

Therefore, gaining a deeper understanding of pilot spray atomization and

its transient behavior could be crucial in ensuring optimal performance of DF engines, where fuel mixture formation is a critical aspect that significantly affects engine performance and emissions. To study this process, researchers have extensively investigated diesel sprays produced by common-rail injectors with single-hole and multi-hole nozzles in a high-pressure chamber using various visualization methods [9]–[12]. Some have even used custom-made single-hole nozzles, while others have modified multi-hole nozzles into single-hole nozzles by micro-welding to investigate the single spray plume [13].

Single-hole nozzles are often preferred in experimental research because they offer better optical observation and simpler parameter adjustment compared to multi-hole nozzles. Despite this, multi-hole nozzles remain the standard solution for practical engine applications [14]. Apart from that, single-hole nozzles are especially advantageous for single spray plume analysis, as they avoid issues with adjacent plume interference in the optical setup. But, the study by [14] found that, under the same rail pressure condition, a single-hole nozzle injector spray could produce more extended penetration than that of a multi-hole nozzle injector. The evaporation rate and mixture formation process of the single-hole nozzle injector were inferior to those of the multi-hole nozzle injector. This could be due to the faster pressure build-up inside sac volume [9]. Also, [15] reported that the location of the holes is a critical factor that directly affects the flow inside the sac volume. Therefore, to limit any nozzle modifications, [16] utilized a thimble concept similar to a cap-like structure placed on top of the injector nozzle. This thimble isolates the single spray plume from the multi-hole nozzle spray.

Pilot sprays are small amounts of fuel that are injected at low needle lift conditions, which makes them highly sensitive to injector transitional behaviour. Understanding the characteristics of these transient sprays is crucial for optimizing direct pilot fuel ignition and combustion. Therefore, the study employed two concepts: a thimble and blocking the nozzle holes, to investigate isolated spray plumes. The resulting sprays from these concepts are referred to as plume-thimble and plume-blocking, respectively. Additionally, the study examined the spray characteristics of a multi-plume to investigate plume deviation among plume1-9, as it is a nine-hole nozzle (with all holes open). Furthermore, it explored the advantages of using the thimble method compared to blocking under various atmospheric and injection pressure conditions.

Meeting the stringent emission regulations imposed on modern combustion engines poses a challenge for engine designers. To address these standards, engineers have been researching to develop innovative techniques and integrate them with existing engine subsystems to reduce pollutant emissions. One such subsystem is the fuel injection mechanism, which has shown potential for development, resulting in improved engine performance and emission quality. This progress is achieved through enhanced control of the fuel injection process. Ultimately, the quality of the fuel spray and its distribution within the combustion chamber determines the combustion efficiency. The spray characteristics, especially spray penetration length, cone angle, and area, have been extensively investigated in the literature, often using constant volume [17], [18] and constant flow chambers [19], [20] to replicate in-cylinder thermodynamic conditions.

Examining the macroscopic fuel spray characteristics, the breakup and dispersion of the spray are primarily influenced by conditions within the cylinder. These conditions most commonly include ambient density, and temperature, alongside factors such as injection pressure and fuel properties. Furthermore, the geometrical properties of both the nozzle and the injector also contribute significantly to this phenomenon [21]. Increasing ambient density significantly influences spray characteristics. As a result, there is a reduction in spray penetration length due to increased air resistance. This leads to smaller spray areas as particles spread less and a wider spray cone angle, which facilitates a more dispersed spray pattern [22]. Conversely, a study conducted by [23], found that increasing the injection pressure improved the spray tip penetration, spray area.

1.2 Objective

The primary objective of this thesis is to comprehensively investigate the dynamics of transient sprays in internal combustion engines, utilizing essential optical methods such as Mie-scattering and diffuse backlight imaging to meticulously scrutinize spray morphology and enhance our comprehension of combustion processes. In order to achieve this goal, the study adopts two distinct yet complementary methodologies: one employing a thimble-equipped nozzle and the other a plume-blocking approach. These methodologies facilitate an in-depth examination of a multi-hole diesel fuel injector within a constant-volume spray chamber. While the thimble-equipped nozzle yields outcomes closely resembling those of a standard nozzle, the plume-blocking approach showcases distinctive rapid penetration characteristics, although it may have limitations in single-spray studies. Additionally, the research extends its scope to include a systematic analysis of diesel injector sprays sourced from various manufacturers. It aims to examine the influence of manufacturing variations, notably hole dimensions, on spray and mixing processes. Through carefully conducted experimental evaluations under diverse injection conditions, including variations in ambient gas densities injection pressures, the study aims to elucidate critical factors that impact spray behaviour using RMSE metrics. Moreover, it seeks to enhance the precision and accuracy of computational models for assessing diesel injector performance.

1.3 Organization of the thesis

In the introductory Chapter 1, we provide the context and purpose of the research. Chapter 2 details the materials and methodologies used, forming the basis for subsequent experimentation. Chapter 3 shifts the focus to spray analysis at ambient temperatures, while Chapter 4 extends the investigation to analyze sprays under increased temperatures. Finally, in Chapter 5, we present and discuss the results, connecting the findings from Chapters 3 and 4 to draw meaningful conclusions and insights into the research topic.

Chapter 2

Materials and methods

2.1 Nozzles and injection system

The fuel delivery system is vital for providing fuel at the right pressure and rate. It has two main parts: a hydraulic fuel pressure enhancer and a fuel supply line. The fuel supply line includes an electronic pressure regulator and a pressure sensor to control injection pressure. During each 10-second cycle, the fuel pressure depends on the system's hydraulic pressure and goes to the injector. We used a marine diesel injector with a nine-orifice nozzle, and its parameters are in Table 2.1. The injector was kept at a consistent temperature of about 300 K (room temperature) for all lab tests. For the experiments, we used a commercial light fuel oil (LFO) with a density of 833.5 kg/m^3 (at 15 °C) and a kinematic viscosity of 3.036 mm^2/sec (at 40 °C) as our fuel.

Injector name	Size of the nozzle orifice (⌀) (mm)	Number of holes
A1	0.31	9
A2	0.31	
B	0.32	
C	0.365	

Table 2.1: This table offers information on the injectors utilized in the research, including the dimensions of their nozzle openings and the quantity of holes in each one.

2.2 Strategies for isolating spray plumes

To study a single spray plume without interference from the multi-plume created by a multi-hole nozzle, two distinct methods were employed. The first method involved blocking or sealing off all other nozzle openings, leaving only one open for use as shown in Fig.2.1(c). This resulted in the creation of what we call a "plume-blocking" spray. The second method entailed designing a thimble

attachment for the nozzle, as illustrated in Fig.2.1(a). This design allowed only one spray plume, referred to as "plume-thimble" to enter the chamber, while all other plumes were collected and drained. The injector was positioned at an incline at the bottom of the chamber, as depicted in Fig. 3.2, ensuring that collected fuel flowed directly into the chamber's drain. Additionally, precise control over the timing of the thimble drain valves was implemented after each injection cycle to prevent any increase in fuel pressure within the drain passages or the thimble itself. The ninth hole was specifically selected for the thimble method, ensuring that the ninth plume (known as "plume9") was directed into the chamber, while the thimble gathered the remaining plumes. For a visual reference indicating plume/hole numbering and orientation, please consult Fig. 2.1(b).

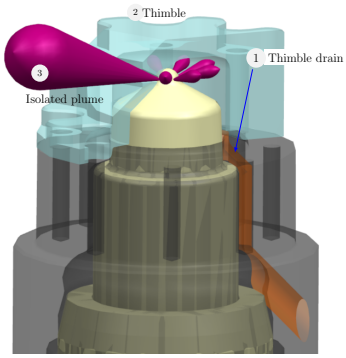

(a) Thimble cad design.

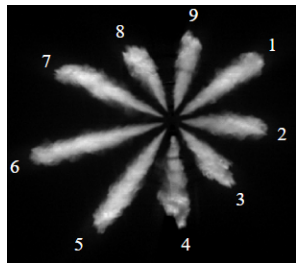

(b) Close-up view of an isolated nozzle orifice.

(c) Sealed (micro-welding) nozzle.

Figure 2.1: Illustrated here are plume isolation methods. (a) Demonstrates the thimble design, a specialized attachment that isolates one spray plume while redirecting others. (b) illustrates the arrangement and numbering strategy for multiple plumes. (c) Displays a sealed (micro-welding) nozzle modification for plume isolation.

2.3 Test conditions

A range of diverse test conditions were deliberately chosen to gain a thorough insight into spray characteristics. Test conditions were carefully selected to investigate the pilot spray's complete behavior. The experiment involved

the examination of specific test points, detailed in Table 2.2. These chosen conditions aimed to faithfully replicate the thermodynamic aspects pertinent to large-bore engines while also shedding light on how these pilot sprays affect engine performance in transient scenarios.

Test Matrix	
Nozzle Setup	Multi-hole, Blocked, Thimble
Chamber Density (kg/m^3)	14.62, 27.69
Temperature (K)	300
Fuel Pressure (MPa)	170, 210
Injection Duration (μs)	500

Table 2.2: Test Matrix Conditions and Nozzle Setup.

2.4 Spray visualization test rigs

Optical test rigs designed for spray research are deployed globally in both academic and industrial settings. Their primary objective is to replicate ambient conditions resembling those in actual engines during fuel injection and combustion. This includes emulating high-pressure, high-temperature scenarios similar to diesel engines at the top dead centre (TDC) and maintaining near-atmospheric pressure conditions for gasoline direct injection (GDI) spray studies. Different types of such test rigs are employed worldwide, each serving specific purposes. Here is a brief overview of these rig types. In fuel spray research, optical test setups play a pivotal role in replicating the conditions present in a real engine, particularly just before fuel ignition at the piston's top dead centre. One such setup that closely mimics an engine is the Optical Research Engine (ORE). OREs typically feature a single-cylinder design with accessible combustion chambers through various window configurations. However, optical accessibility in OREs is limited, especially when examining fuel spray interactions with cylinder components [24], [25].

Another category of test rigs is the Rapid Compression Machine (RCM) discussed by [26]. Through the use of a single compression stroke, RCMs are engineered to attain the necessary pressure and temperature conditions at the top dead centre (TDC). Subsequently, they enable the visualization of combustion within the cylinder through constant-volume processes. Nevertheless, RCMs come with substantial fabrication costs and operational complexities. Notably, the vibrations at the end of the compression stroke present challenges when conducting measurements using diverse laser-based optical diagnostic techniques. On the other hand, the Constant Pressure Flow Test Rig (CPFR) is a high-pressure and high-temperature chamber. Within this setup, a compressor pressurizes and stores gas within a high-pressure reservoir. Subsequently, the gas flows continuously through the test rig. Before entering the test rig, electric resistance heating is applied to elevate the gas temperature. The versatility of the CPFR lies in its ability to operate in both open- and closed-loop systems according to the specific requirements of an experiment [20].

The final two types of test rig systems belong to the category of constant volume chambers. These chambers are designed to isolate a specific quantity of oxidizers, typically air or oxygen, and are constructed to withstand high pressures and temperatures. Fuel is then introduced into this heated and pressurized chamber, initiating oxidation, which facilitates the study of both the spray and combustion processes. Alternatively, the chamber can be filled exclusively with inert gas for a focused examination of the fuel spray. This chamber type stands out due to its precise control over temperature and pressure parameters. Firstly, there's the Constant Volume Hot Cell (CVHC), which features a simple design employing a heating element to elevate gas temperature. However, this simplicity imposes pressure limitations due to material stress caused by high temperatures, potentially causing combustion disruptions. For achieving the desired pressure, high-pressure gases (inert for spray studies and air for combustion) are employed in conjunction with the heating element. Fuel injection takes place once the necessary conditions are met. Drawbacks include the risk of O-ring damage, mandating injector cooling, and an upper-temperature limit constrained by heating material restrictions [12], [27]. Secondly, focus on the Constant Volume Pre-combustion Cell (CVPC). The desired pressure and temperature levels are generated within this chamber by igniting a lean gas mixture. Subsequently, the fuel spray is introduced into the residual combustion area, where oxidation occurs. This technology enhances the chamber's versatility, with further details provided in the pre-combustion section. Importantly, this chamber is well-suited for conducting experiments at high pressures and temperatures, explaining its widespread use in modern research settings [20].

Various types of optical test rigs are available, with ORE and RCM being particularly similar to conventional engines. Choosing the most suitable test rig depends on specific research goals, factors impacting results, and budget limitations. Different test rigs are ideal for different purposes. This current research employs the Constant Volume Pre-combustion Cell (CVPC) to investigate spray characteristics. The features of the spray chamber are elaborated upon in the following sections.

2.4.1 Optical Spray Combustion Chamber (OSCC)

The experimental trials took place within the Optical Spray Combustion Chamber (OSCC) confines. This chamber, designed as a pre-burn constant-volume spray enclosure, incorporates a fused silica window, affording optical access from multiple vantage points. The OSCC system's blueprint was influenced by a prior spray chamber concept introduced by [9] in their research work. The experimental investigation was designed into three distinct phases, each carefully structured to address specific aspects of spray behaviour. During the initial phase, the chamber was dedicated to studying non-evaporative and non-reactive sprays, emphasising maintaining ambient temperature conditions at 300K while systematically adjusting ambient pressures. In the subsequent second phase, the research shifted its focus to evaporating and non-reactive sprays, which involved elevated temperatures exceeding ambient levels and

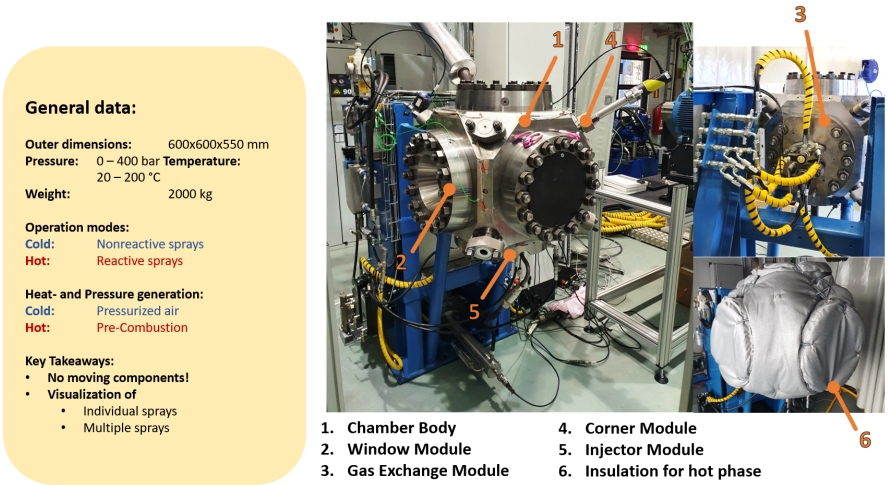

Figure 2.2: A detailed graphical overview of the Optical Spray Combustion Chamber (OSCC) features its multi-phase design equipped for comprehensive spray testing across non-reactive and reactive spray experiments..

precise control of ambient pressures. In the third and final phase, the study examined evaporating and reactive sprays, characterised by various temperature and pressure conditions that went beyond ambient levels. The licentiate thesis primarily emphasises the results obtained from the first phase, explicitly dealing with non-evaporative and non-reactive spray experiments. In the initial experimental phase, the chamber was pressurised using air to attain the required ambient density while maintaining the temperature at ambient levels. In contrast, for the subsequent second and third phases, the desired pressure and temperature conditions were achieved by using a pre-combustion technique.

Chapter 3

Spray analysis in ambient temperatures

Examining spray under atmospheric temperature i.e non-reactive and non-evaporative sprays in diesel engines sheds light on the early stages of fuel injection and dispersion before combustion. When diesel is propelled into the combustion chamber, it typically forms a spray to enhance mixing with air, an essential step for effective combustion. However, before reaching the combustion area, the fuel remains non-reactive and non-evaporative, meaning it does not engage in chemical reactions or turn into gas. Exploring the spray during this initial phase provides insights into how fuel breaks up, spreads, and interacts with the surrounding environment, which is vital for boosting engine efficiency and curbing emissions. By scrutinizing non-reactive and non-evaporative sprays in diesel engines, it is possible to tweak injection settings, like the timing and pressure of injection, to secure desired spray traits that lead to improved combustion efficiency and lowered emission rates. The mie-scattering technique was used to study multi-plume spray while Diffuse back light imaging has been utilised to capture single-plume spray respectively under atmospheric temperature with variable ambient pressures. The chamber was pressurised using air to attain the required ambient density while maintaining the temperature at ambient levels. Two distinct spray

Operation Modes	**Spray Configuration**	**Imaging Methods**
Non-reactive & non-evaporative	Multi-plume	Mie-scattering
	Single-plume (plume-blocking & plume-thimble)	Diffuse back-light

Table 3.1: Operation modes and corresponding optical techniques.

configurations are employed in the Non-reactive and non-evaporative modes: Multi-plume and Single-plume. The Multi-plume configuration is analyzed using the Mie-scattering imaging method, which is known for its effectiveness

in capturing scattered light from particles within the spray. On the other hand, the Single-plume configuration is further categorized into two setups: plume-blocking and plume-thimble, both of which are analyzed using the Diffuse back-light imaging method. The optical visualisation methods utilised are listed in Table.3.1.

3.1 Mie-scattering

Two distinct imaging methodologies were employed to investigate non-reactive and non-evaporative spray: the Mie-scattering technique for multi-spray observation and the back-lighting technique for single-spray examination, which is called plume-blocking and plume-thimble. To ensure adequate illumination during Mie-scattering, LED lights (Veritas's constellation 120E) were strategically positioned on either side of the spray chamber, providing uniform lighting for plume visualization, as depicted in Fig. 3.1. The injector, located at the bottom of the chamber, was oriented vertically, and image capture occurred from the top plane. The synchronization of the light source and imaging devices allowed for automatic light intensity adjustment, maintaining a consistent level based on frame rate and exposure time.

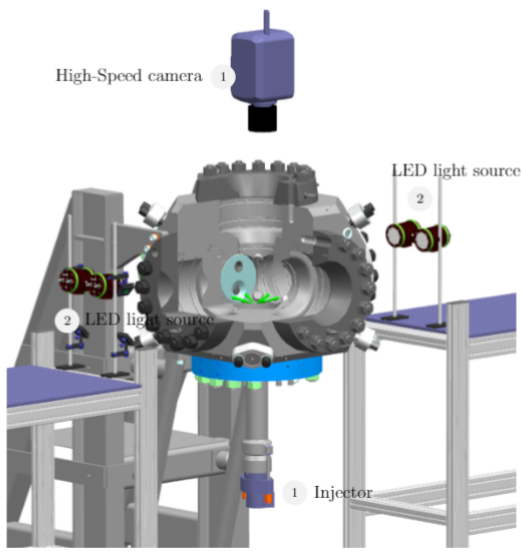

Figure 3.1: Schematic representation of Mie-scattering optical configuration.

3.2 Diffused back-illumination imaging (DBI)

Additionally, the study incorporated the use of back-lighting as an alternative illumination method, a common choice for liquid-phase measurements and

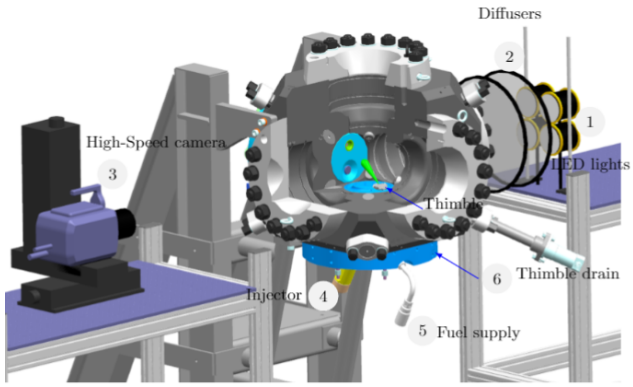

Figure 3.2: Schematic representation of diffuse backlight (DBI) configuration.

visualization experiments. In this setup, the light source and imaging device were aligned in the same direction, positioned opposite each other, as illustrated in Fig. 3.2. For both Mie-scattering and back-light imaging, a high-speed CMOS camera equipped with a Micro NIKKOR lens was employed to capture spray events. This specialized lens boasted a 105mm reach, a maximum aperture of f/2.8, and a 1:1 reproduction ratio, ensuring the acquisition of precise and highly detailed spray images. Specifically, the imaging process involved capturing images at a rate of 35,000 frames per second, with a resolution of 512×512 pixels and exposure times of 9 and 3 microseconds for Mie-scattering and back-light imaging, respectively.

3.3 Spray contour detection procedures

This research utilized custom MATLAB code for applying image processing and contour recognition techniques to digital photos. The initial image processing steps differ based on the type of image, encompassing Mie-scattering, diffuse back-light, shadowgraph, and Schlieren images. Nonetheless, once the spray contour is successfully identified, the subsequent steps remain consistent across all image types to extract spray characteristics. A detailed explanation of the step-by-step procedure is provided in the following sections for a more comprehensive understanding of the process.

Multi-plume spray: The Mie-scattering technique is utilized to visualize multiple sprays under ambient conditions, specifically referring to non-reactive and non-evaporative sprays. This technique is illustrated in Fig. 3.1.

Step-I: Initially, an image taken before injection was subtracted from the spray image to remove reflections and background anomalies. In the case of Mie-scattering, the background image (see Fig.3.3(a)) was subtracted from the original spray image (see Fig.3.3(b)) to eliminate background noise. The resulting subtracted image is presented in Fig.3.3(c). ***Step-II:*** The adjusted image (Fig. 3.3(c)) was then converted to a binary format using Otsu's

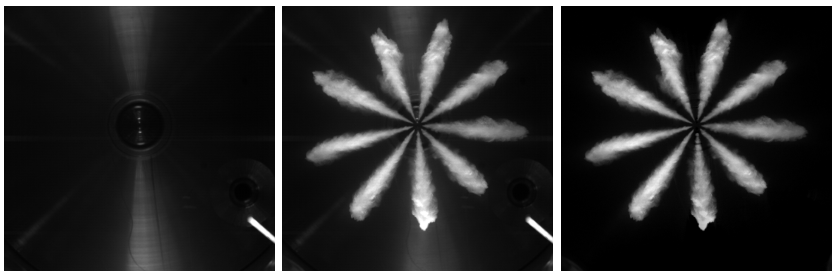

(a) Back-ground image (b) Original image (c) Subtracted image

Figure 3.3: Output of background removal process

algorithm [28], the resulted image as shown in Fig. 3.4.

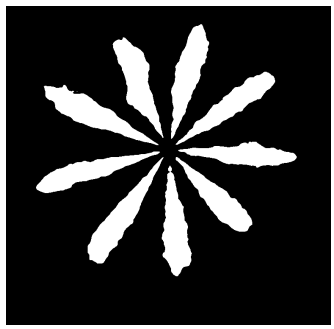

Figure 3.4: Binary image.

Step-III: Subsequently, a masking technique [29]–[31] was utilized to split the multi-spray image into distinct segments, each corresponding to a single plume, thereby enabling separate analysis for each plume. The result of masking is illustrated in Fig. 3.5, showing the appearance of plume-1 post-masking technique. The angle of the central axis for each plume was measured relative to the horizontal line, and the plumes were then rotated to a vertical orientation to simplify the coding process. Fig. 3.6 shows the rotated plume-1. A similar procedure is applied to the rest of the spray plumes to extract and rotate them vertically.

Step-IV: In the final stage, metrics such as penetration length, surface area, and spray cone angles were determined for each plume. A thorough explanation of the procedure employed for calculating these spray characteristics is provided in the following sections.

Single-plume spray: The diffuse back-light imaging technique was employed to visualise single-plume spray. The post-processing of these images follows a similar procedure as discussed for Mie-scattering images, but with a few minor differences, the steps are as follows.

Step-I: Unlike in Mie-scattering, where the background image was subtrac-

Figure 3.5: Isolated plume-1 after masking.

Figure 3.6: plume-1 after rotating vertically.

Figure 3.7: Illustration of the masking technique applied to plume-1 (left), and the subsequent rotation to a vertical orientation (right).

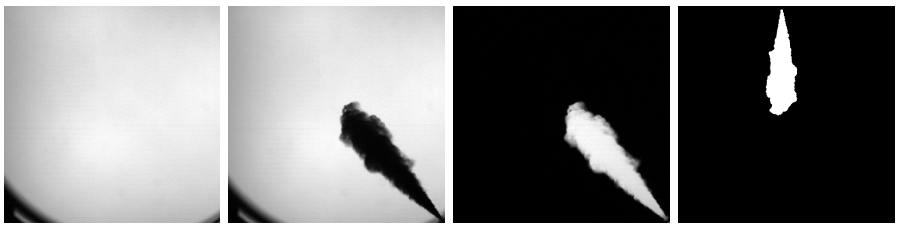

(a) (b) (c) (d)

Figure 3.8: Processing steps in back-light images: (a) Background image, (b) Spray image, (c) Subtracted image, (d) Binary image and rotated

ted, here, the spray image is subtracted from the background due to higher pixel intensities compared to those within the spray. ***Step-II:*** The adjusted image (Fig. 3.3(c)) was then converted to binary format using Otsu's algorithm [28], as shown in Fig. 3.4. ***Step-III:*** Upon conversion to binary, the single-plume spray is directly rotated to a vertical orientation without masking to calculate spray characteristics. The segmentation algorithms utilized are discussed in-depth in the cited literature [32]–[34]. Once the images are converted into binary, the procedure to calculate spray characteristics remains the same, as discussed below.

Spray penetration length and area

The evaluation of spray penetration is commonly carried out directly by measuring the axial span between the nozzle outlet and the farthest point of the spray [23], [35]. For uniformity, the length of spray penetration is delineated as the distance from the spray tip along its axis to a line encompassing 99% [36] of the spray area, depicted in Fig. 3.10. Within the binary image of the spray, the spray area is deduced by totalling all pixels with a value of one. Utilizing the mm/pixel ratio, the measurements of spray penetration (pixels)

and area ($pixels^2$) are transposed into mm and mm^2, respectively. The relevant equations are stated below,
Length of Spray Penetration (S):

$$S(mm) = S(pixels) \times mm/pixels \tag{3.1}$$

Area of Spray (SA):

$$SA(mm^2) = A(pixels^2) \times (mm/pixels)^2 \tag{3.2}$$

In scenarios employing a thimble, a segment of the spray area is obscured by the thimble can be seen in Fig. 3.9, rendering it impractical to omit it during the calculation of the total spray area. Consequently, an equivalent area ($SA_{equivalent}$) was incorporated into the measured area as calculated based on the Eq. 3.2, leading to the final equation, Spray Area in the presence of a thimble ($SA_{plume-thimble}$)

$$SA_{plume-thimble}(mm^2) = SA_{measured} + SA_{equivalent} \tag{3.3}$$

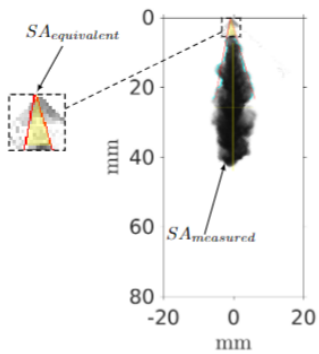

Figure 3.9: Spray area hidden by thimble thickness.

Spray cone angle

Determining the spray cone angle accurately is crucial, and one effective method involves measuring the angle formed by two lines fitted along the spray boundary edges. These lines are determined through a least-square fitting process and can be located either close to or far from the spray source. The distance they cover is typically related to the spray penetration length or multiples of the nozzle orifice diameter (D). Ideally, these lines can extend up to the nozzle tip coordinates, where they may intersect or remain separate, leading to different cone angle calculations in each case. The choice between these methods must be well-justified. This article delves into the factors influencing the selection of one method over the other, with consideration for the nozzle tip and spray

origin coordinates. In the first approach, the cone angle is computed by fitting lines from the spray origin to a distance proportional to the spray penetration length (usually around 60-70% of S) [33], [37], [38]. A least-square fitting technique is applied to find the best-fit lines, similar to the triangle criteria proposed by [17], [39]–[41]. Researchers have widely adopted this approach and have defined the penetration distance as a function of the injector orifice diameter, spanning a range from $10D$ to $100D$ [32], [42], [43].

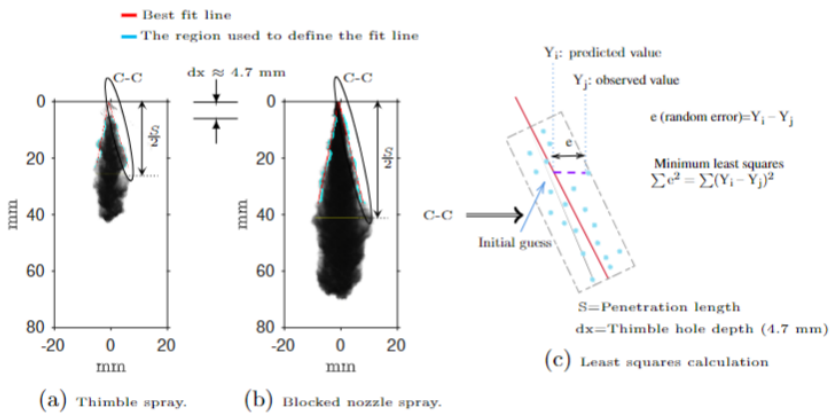

Figure 3.10: Cone angle measurement.

In the second approach, lines are fitted between two points on the spray contour without being fixed at the origin. These points are strategically chosen to encompass the region of interest within the spray. This method proves effective when acquiring the spray contour is challenging or when the region near the nozzle lacks significance [44], [45]. Our study determined the cone angle by modifying the first approach discussed earlier. Initially, we detected the spray boundary using binarization and drew an initial fitted line within the spray contour, anchoring it at the spray origin (see Fig. 3.10c). The line then moved progressively toward one side of the spray edge, and at each step, we calculated the least-square error (at each pixel position). This process continued until the least square value reached its minimum, as shown in Fig. 3.10c. Similarly, we applied the same procedure to identify the fitted line on the opposite side of the spray edge, and the angle between these lines was then defined as the cone angle for that specific spray. Our experimental setup included a thimble that concealed the initial spray up to a thickness of 4.7 mm. Consequently, we could not utilize the spray boundary within the thimble when computing least squares. However, we positioned the spray contour between the thimble exit and selected 60% of the spray penetration length to calculate the least square error. To maintain methodological consistency and mitigate potential variations in cone angles arising from different approaches, we excluded the spray below 4.7 mm from the nozzle tip in calculating cone

angles for plume-blocking and multi-plume sprays (plume1-9). In all cases, the fitted lines were drawn from a virtually fixed spray origin (see Fig. 3.10), which coincided with the nozzle tip.

Chapter 4

Spray analysis at increased temperatures

In modern optical constant volume chambers, pre-combustion technology is now frequently employed to study fuel spray under elevated temperature and pressure conditions. The ongoing research uses the pre-combustion technique to achieve the desired pressure and temperature settings. Within these studies, careful control over the oxygen (O_2) level remaining after combustion is exercised for analyzing non-reactive and evaporative sprays, and reactive sprays.

4.1 Pre-combustion

The pre-combustion process involves a sequence of steps, including chamber evacuation using a vacuum pump, followed by a controlled gas injection to achieve the desired mixing ratio. This results in a lean gas mixture, which is then ignited by a spark, and the chamber's pressure is closely monitored. The correct gas mixture is determined by measuring pressure changes during gas release. Each gas contributes a predetermined partial pressure based on its volume percentage in the mixture. As the lean gas mixture ignites, pressure and temperature levels within the chamber begin to rise. This ignition process results in a noticeable pressure peak inside the chamber, as visually demonstrated in Fig. 4.1. Subsequently, pressure gradually declines as the heat generated by combustion disperses through the chamber walls. Once the desired pressure and temperature are reached, fuel spray injection takes place. The actual pressure and temperature at the time of injection was measured using sensors located at the corner modules of the chamber. The Fig.4.2 presents a representative view of the measured pressure and corresponding temperatures data.

The selection of gases requires consideration of combustion byproducts and ignition properties, particularly due to the gas mixture's oxygen-rich nature. In the current research, hydrogen and air mixtures are utilized to investigate

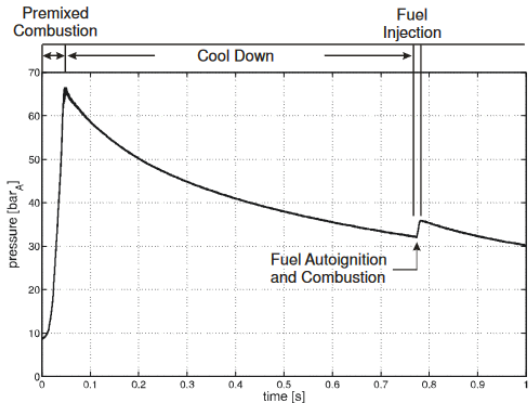

Figure 4.1: A schematic representation illustrating the fundamental operation of pre-combustion concept [9].

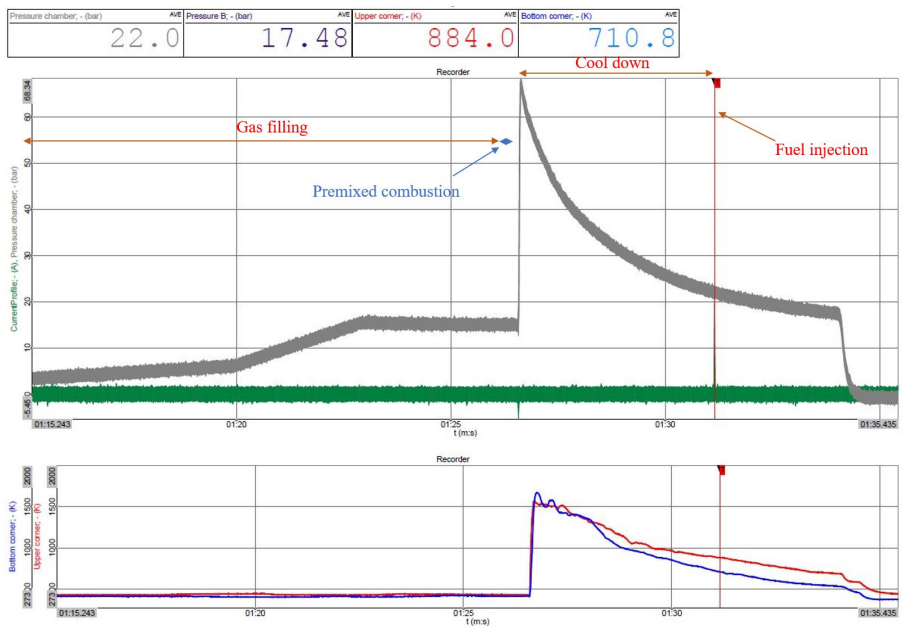

Figure 4.2: A schematic representation illustrating the pressure and temperature data from test.

spray evaporation under non-reactive conditions, aiming for 0% oxygen product volume at the end of the pre-combustion. However, a specific percentage of oxygen is added for the study of reactive spray. Detailed information about the gas mixtures employed in this study to achieve the required pressure and temperature can be found in the Table. 4.1 and Table. 4.2. It's important to note that the exclusive use of hydrogen helps eliminate carbon dioxide in

combustion residues but may lead to excessive water vapour after compilation of pre-combustion, potentially causing condensation on the chamber windows. To address this concern, the chamber walls are maintained at approximately 120 °C to prevent adverse effects. The licentiate thesis primarily emphasises the results obtained from the first phase, explicitly dealing with non-evaporative and non-reactive spray experiments.

Target Pressure (bar)	**Density (kg/m^3)**	**Target Temperature (K) ±25**	**H_2 (bar)**	**Air (bar)**	**O_2 (bar)**	**N_2 (bar)**	**Lambda**	**%O_2 after Combustion**
23	14.38	800	3.71	8.829	0	3.971	1	0
29		1000	3.71	8.829	0	3.971	1	0
33	19.76	800	4.29	10.21	0	8.18	1	0
43.5		1000	4.29	10.21	0	8.18	1	0
46	27.24	800	6.658	15.845	0	8.777	1	0
57		1000	6.658	15.845	0	8.777	1	0

Table 4.1: Summary of target pressure, temperature, and gas composition for non-reactive and evaporative sprays.

Target Pressure (bar)	**Density (kg/m^3)**	**Target Temperature (K) ±25**	**H_2 (bar)**	**Air (bar)**	**O_2 (bar)**	**N_2 (bar)**	**Lambda**	**%O_2 after Combustion**
30	14.38	850	1.8	13.712	1	0	3.2	19
40.5		1150	1.8	13.712	1	0	3.2	19
42	19.76	850	2.605	18.601	1.5	0	3	19
54		1150	2.605	18.601	1.5	0	3	19
56	27.24	850	3.411	25.978	1.9	0.003	3.2	19
71		1150	3.411	25.978	1.9	0.003	3.2	19

Table 4.2: Summary of target pressure, temperature, and gas composition for reactive sprays.

Shadowgraphy and Schlieren imaging methods are employed to analyze the spray characteristics for the Non-reactive and evaporative modes. On the other hand, the reactive mode utilizes three different imaging methods: Shadowgraphy, Schlieren, and Luminosity. These imaging techniques enable a thorough analysis of the spray behaviour under different combustion scenarios. Table.4.3 representation efficiently categorizes and presents the varying configurations and imaging methods.

Operation Modes	**Spray Configuration**	**Imaging Methods**
Non-reactive & Evaporative	Single-Plume (Thimble)	Shadowgraphy Schlieren
Reactive	Single-Plume (Thimble)	Shadowgraphy Schlieren Luminosity

Table 4.3: optical techniques for analysing sprays at increased temperature.

4.2 Shadowgraph and Schlieren imaging

Shadowgraph and Schlieren's methods are key to identifying boundaries with refractive index gradients. When a collimated beam illuminates such an environment, some rays are deflected, creating varying shades in the image, while others remain undeflected, forming a uniform background [46].

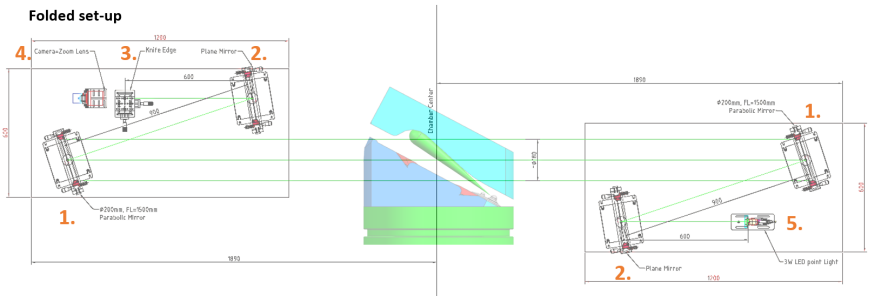

Figure 4.3: Experimental setup illustrating the arrangement of optical components. The setup includes: (1) Parabolic Mirrors (2 number), (2) Plane Mirrors (2 number), (3) Knife Edge, (4) High-speed Camera equipped with a Micro lens, and (5) Point light source (laser).

The boundary exhibits a different refractive index in evaporating sprays due to the vaporized fuel and ambient gas, with evaporative cooling causing density and temperature gradients [47]. These techniques help elucidate the vapour boundary. The needed equipment includes a point light source, large collimating and collecting optics, an imaging lens, and high-speed cameras. The optical setup in Schlieren imaging is similar to shadowgraphy but uses a spatial filter, typically a knife-edge, to block some light from the test section. A simplified schematic is in Fig.4.4 shows shadowgraph (left) images for evaporating, non-reacting sprays. In non-reactive tests, the background image intensity is steady before injection due to weak ambient gas turbulence in the chamber, while reactive sprays (right) show a textured background in Schlieren images due to ambient density and temperature fluctuations.

4.2.1 Spray contour detection of shadowgraph and Schlieren images

In the context of evaporating and reactive sprays, a noticeable texture in the shadowgraph and Schlieren images can be attributed to surrounding density and temperature variances, as illustrated in Fig.4.4. The tracing of the spray boundary is obtained from the intensity difference between consecutive images [47], [48]. Utilizing Otsu's algorithm [28], the threshold value applied for image binarization and, consequently, spray boundary determination is computed (see Fig. 4.4). The area within the defined spray boundary defines the spray's projected area. The length of the spray encapsulating 99% of the projected spray area is termed as the vapour penetration length.

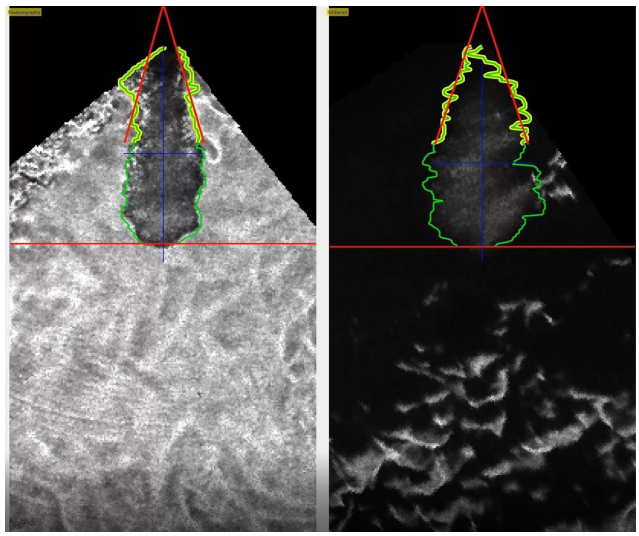

Figure 4.4: Spray contour detection showcasing the derived measurements of cone angle and spray penetration length, as captured by shadowgraph (left) and Schlieren (right) techniques.

4.3 Natural luminosity

The Natural Flame Luminosity optical method is a pivotal technique for studying the dynamics of diesel spray combustion. The high-speed colour camera captures the luminosity emitted when fuel spray ignites. The combustion process of the spray was meticulously recorded under various temperatures and ambient densities, with differing oxygen concentrations present at the time of injection. The method provides a clear visual representation of the combustion process, as well as an insight into how temperature, density, and oxygen concentration interact during the combustion of diesel spray, particularly low and high temperature combustion situations.

Chapter 5

Results and discussions

The report is organized into four distinct sections, each aimed at providing a comprehensive grasp of the research. In the first section, our focus centres on evaluating the effectiveness of plume isolation under different ambient density conditions. Specifically, we emphasize the performance of plume-thimble and plume-blocking sprays across various ambient density levels. Moving to the second section, we compare plume-thimble behaviour with that of plume-9, which is derived from a multi-plume spray. Plume-9 is chosen for analysis because it originates from the same orifice hole as a nozzle fitted with a thimble. This comparison helps us determine whether the presence of the thimble consistently affects the spray. In the third section, our analysis shifts to examining variations among the multi-plume sprays, spanning from plume-1 to plume-9, and comparing them to the results obtained from plume-thimble and plume-blocking. Throughout this section, we maintain our focus on key spray characteristics, including spray penetration (S), spray area (SA), and spray cone angle (θ), all directly measured from the spray images. The graphs in this section present the average findings from fifteen spray events, with shaded areas around the data points to ensure precision and reliability. The results from sections one to three are reported in paper one, while paper two focuses on the results of section four.

Concluding the report, the fourth section addresses concerns arising from inconsistent performance due to manufacturing variations in diesel injectors. This section thoroughly examines sprays from four distinct injectors, encompassing a wide range of injection conditions, including varying ambient gas densities and injection pressures. To investigate variations in spray penetration length among the injectors, we utilize Root Mean Square Error (RMSE) analysis, which provides valuable insights into both symmetric and asymmetric spray behaviours.

5.1 Summary of Paper-I

5.1.1 Comparison of plume-thimble, plume-blocking and plume-9

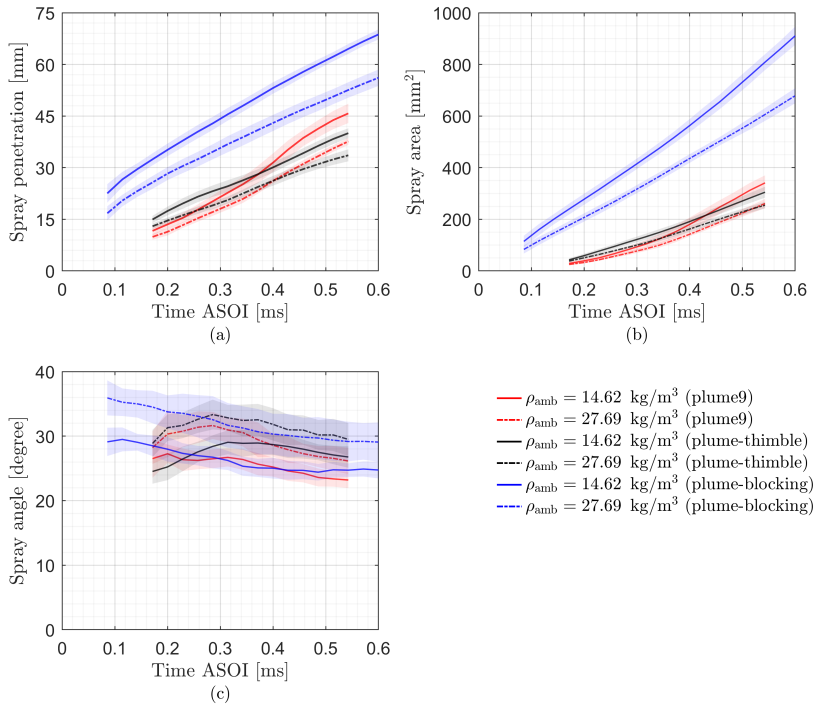

Figure 5.1: Comparison of Spray Characteristics: Spray penetration, spray area, and spray cone angle (θ) for plume-thimble, plume-9, and plume-blocking in various ambient density conditions. The shaded areas around data points indicate precision and repeatability, based on an average of fifteen spray events.

In Fig.5.1a, it's evident that plume-blocking sprays outperform plume-thimble in terms of penetration, indicating that blocking nozzle holes introduces notable changes in the spray dynamics, resulting in faster penetration, these variations can also observed from image sequences in Figs. 5.2 and 5.3. As the ambient density increases, as observed in Fig. 5.1a, b, and c, both the penetration and spray area decrease while the cone angle widens, a phenomenon attributed to the increased energy required for momentum transfer when there is denser gas within the spray. At an ambient density of $\rho_{amb} = 14.62, kg/m^3$, plume-9 initially exhibits a penetration rate similar to plume-thimble, but over time, it diverges, likely due to the stabilizing effect of a thimble near the nozzle tip that reduces fluctuations in spray penetration and area. Injection pressure's impact on spray characteristics, is minimal for plume-9 and plume-thimble,

resulting in no significant deviations in spray area and cone angle. However, plume-blocking displays notable sensitivity to injection pressure, implying a modification in flow distribution within the sac volume due to the blocking strategy. These findings offer valuable insights into the complex interplay between nozzle design, ambient conditions, and spray behaviour, contributing to a deeper understanding of the factors governing spray penetration and angle across different scenarios.

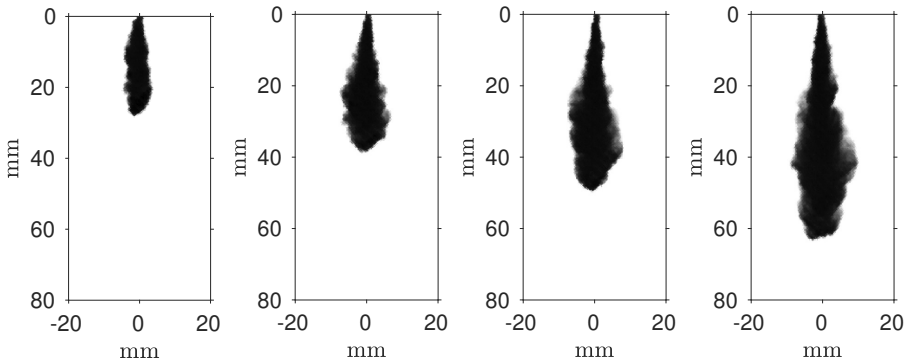

(a) 0.171 ms ASOI (b) 0.286 ms ASOI (c) 0.40 ms ASOI (d) 0.543 ms ASOI

Figure 5.2: Image sequences of plume-blocking at $\rho_{amb} = 14.62\,kg/m^3$, $P_{inj} =$ 210 MPa, $T_{amb} = 298\,K$

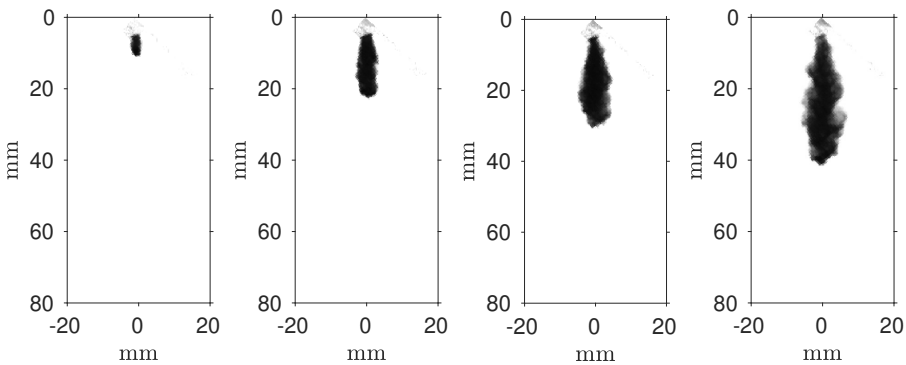

(a) 0.171 ms aSOI (b) 0.286 ms aSOI (c) 0.40 ms aSOI (d) 0.543 ms aSOI

Figure 5.3: Image sequences of plume-thimble at $\rho_{amb} = 14.62\,kg/m^3$, $P_{inj} =$ 210 MPa, $T_{amb} = 298\,K$

5.1.2 Plume to Plume deviation

The application of multi-hole nozzles in injectors introduces variability in fuel injection rates, a parameter that significantly influences the combustion characteristics of diesel engines, leading to heightened emissions and inconsistent

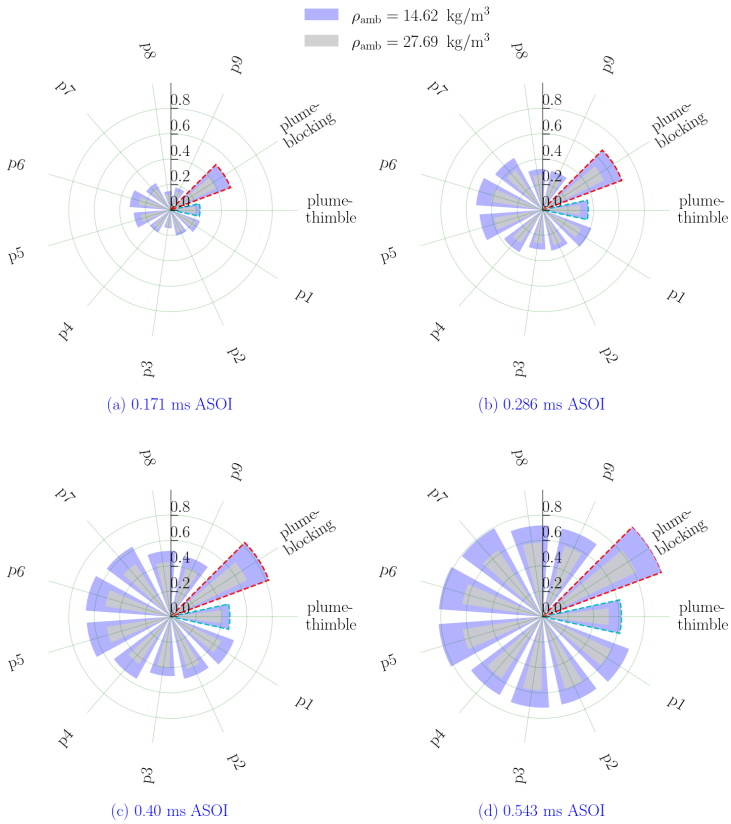

(a) 0.171 ms ASOI (b) 0.286 ms ASOI

(c) 0.40 ms ASOI (d) 0.543 ms ASOI

Figure 5.4: Assessing penetration differences between multi-plume and single-plume configurations (achieved through blocked nozzle and thimble connections) under varying ambient densities..

thermal loads [49]. In order to illuminate the complexities of plume behaviour, this study employs the Mie-scattering technique, as depicted in Fig. 3.1, to comprehensively examine multi-plume sprays. The primary objectives include identifying suitable nozzle orifices for thimble testing and comparing the performance of multi-plume sprays (plume1-9) against that of plume-thimble and plume-blocking sprays. Notably, it is essential to highlight that the test points used in this multi-plume spray analysis correspond to those utilized in thimble and blocking methodologies.

The plumes exhibit significant disparities in penetration, particularly evident at low ($\rho_{amb} = 14.62, kg/m^3$) and high ($\rho_{amb} = 27.69, kg/m^3$) ambient densities, as showcased in Fig. 5.4. Furthermore, variations are observable during the initial stages of the injection process (Fig. 5.4a). However, these discrepancies tend to diminish as the injection progresses (Fig. 5.4d). These deviations are also discernible in the sequence of spray images, as depicted in Fig. 5.5. The root causes of these variations in injection dynamics among nozzle orifices can be attributed to manufacturing imprecision [50] and lateral

oscillations of the injector needle [51]. Notably, [52] underscores that the nozzle orifice closest to the needle displacement experiences more significant obstruction by the needle tip, while the orifice farthest from the needle displacement encounters comparatively less interference, resulting in a larger geometric flow area. Consequently, transient needle movements introduce heterogeneity into the flow distribution within the nozzle orifices, thereby affecting the fuel injection process.

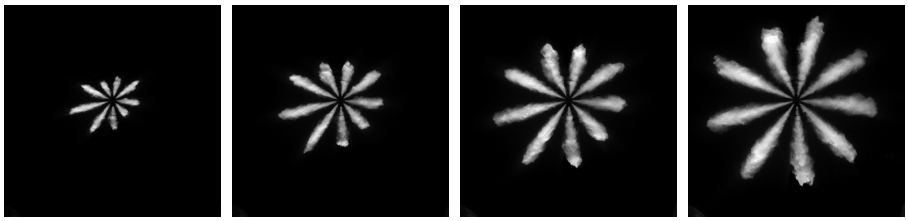

(a) 0.171 ms ASOI (b) 0.286 ms ASOI (c) 0.40 ms ASOI (d) 0.543 ms ASOI

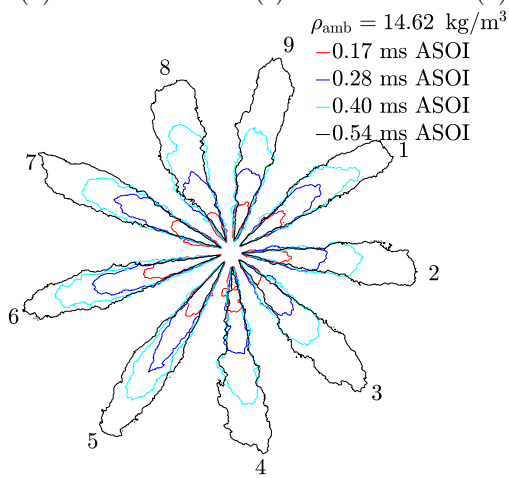

(e) Spray contours

Figure 5.5: Image sequences of multi-plume at $\rho_{amb} = 14.62\,kg/m^3$, $P_{inj} =$ 210 MPa, $T_{amb} = 298\,K$.

5.2 Summary of Paper-II

5.2.1 Manufacturing variations in diesel injector

The Root-Mean-Square Error (RMSE) is a widely used statistical tool for measuring variations within a dataset. In this specific context, it helps us assess how different each plume behaves compared to a reference point known as the averaged plume. The main goal here is to quantify the degree of similarity

or dissimilarity in the behaviour of each plume relative to the overall average behaviour represented by the average plume.

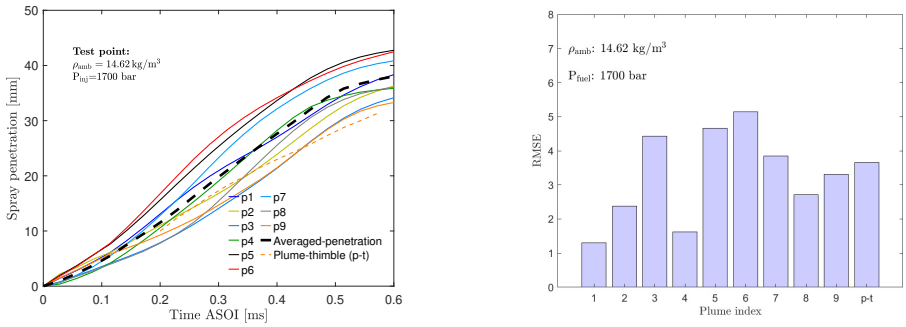

(a) Spray penetration (b) RMSE

Figure 5.6: Fig. 5.6(a) provides a visual comparison of penetration lengths for each individual plume ($P_i(t)$) in contrast to the averaged plume ($P_{\text{avg}}(t)$), represented by the bold solid black line, at the selected test point. On the other hand, Fig. 5.6(b) illustrates the calculation of RMSE with respect to the plume index using Eq. 5.1

The RMSE between each plume and the averaged plume is represented by Eq. 5.1.

$$\text{RMSE} = \sqrt{\frac{1}{n}\sum_{t_1}^{t_2}\left(P_{\text{avg}}(t) - P_i(t)\right)^2} \tag{5.1}$$

Several variables are involved in this analysis. These include n which represents the number of data points, $t1$ and $t1$ indicating the start-of-injection (SOI) and end-of-measurement times, $P_{avg}(t)$, which represents the average penetration length at time t and $P_i(t)$ indicating the penetration length of the ith plume at time t (where i ranges from plume1-9, including plume-thimble (p-t)). The mathematical expression for calculating RMSE, as provided in Eq. 5.1, offers a formula to compute RMSE values for each plume at a given test point. Fig. 5.6 visually presents the RMSE values for each plume at this specific test point. A higher RMSE value indicates more significant differences or variability between each plume and the average plume, while a lower RMSE value suggests that the plume's behaviour closely aligns with the average plume. It is important to note that the thimble hides the initial spray in the case of the plume-thimble. Thus, when calculating the RMSE for the plume-thimble case, we consider only the data points from the average plume ($P_{avg}(t)$) that correspond to plume-thimble (p-t).

RMSE values were systematically analyzed across different ambient and fuel pressure setting combinations for all four injectors: A1, A2, B, and C. This comprehensive investigation aimed to evaluate how injector spray behaviour has been affected by changes in environmental conditions and fuel supply levels. Taking injector A1 as a representative case, as illustrated in Fig. 5.7,

RMSE values were computed for each plume, including the plume-thimble, at various test points. The figure presents two rows of RMSE values: the top row corresponds to an ambient density of 14.62 kg/m^3, while the bottom row represents an ambient density of 26.69 kg/m^3. These calculations were conducted across different fuel pressures, specifically at 1700 bar, 1900 bar, and 2100 bar. This same analytical approach was applied consistently to the remaining injectors, namely A2, B, and Injector C, as elaborated in the subsequent sections.

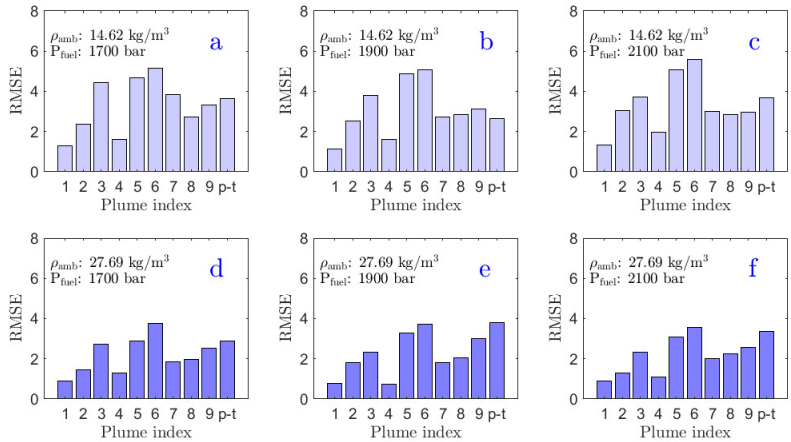

Figure 5.7: Injector A1: RMSE values under different ambient densities (14.62 kg/m^3 and 26.69 kg/m^3) and varying fuel pressures (1700 bar, 1900 bar, and 2100 bar). Sub-figures (a) to (f) in the figure represent the respective test conditions mentioned.

As seen in Fig. 5.7, the RMSE values for the A1 injector reveal significant variations in spray behaviour. Notably, spray plumes 1 and 4 consistently exhibit low RMSE values, closely approximating the averaged plume's behaviour, especially in higher ambient density conditions (26.69 kg/m^3, see Figs. 5.7d-f). This pattern also holds in lower ambient density conditions (14.62 kg/m^3, see Figs. 5.7a-c). Conversely, spray plumes 5 and 6 consistently exhibit high RMSE values across various ambient densities, indicating significant deviations from the averaged behaviour. The remaining spray plumes and the plume-thimble display more distinct patterns, with RMSE values showing variations depending on ambient density. Notably, the RMSE for the plume-thimble closely resembles that of spray plume-9 across all test conditions, likely due to using the 9th hole in the thimble methodology.

To provide a comprehensive overview, we aggregated the RMSE values for each plume across all operating conditions, as depicted in Fig. 5.8(a). This thorough analysis reaffirms the variable performance of all spray plumes, indicating asymmetric spray behaviour regardless of ambient density, whether at 14.62 kg/m^3 or 26.69 kg/m^3. Interestingly, changes in fuel pressure seem to have minimal influence on this diversity, emphasizing the predominant role of ambient density in shaping the injector's performance. These collective RMSE

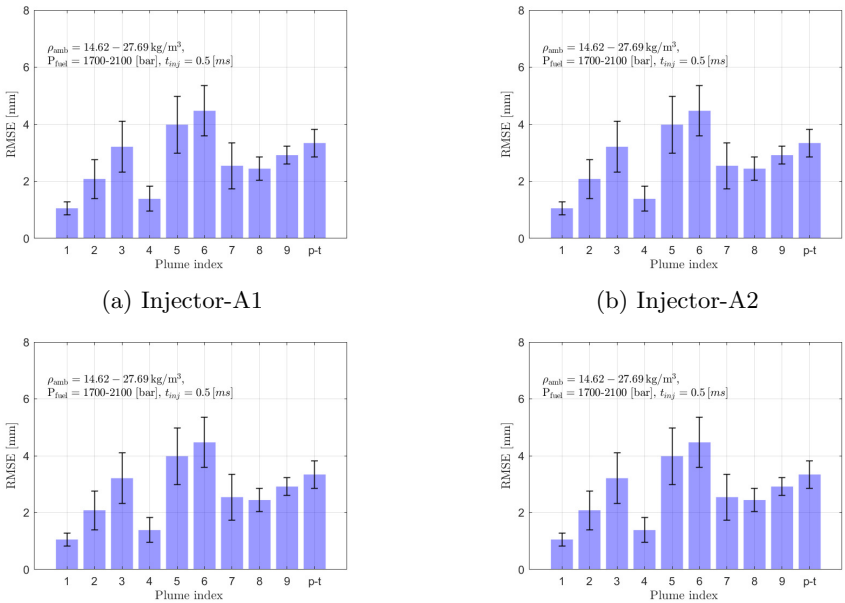

(a) Injector-A1

(b) Injector-A2

(c) Injector-B

(d) Injector-C

Figure 5.8: The sum of RMSE values and their corresponding standard deviations were calculated for each plume across all operating conditions for all four injectors: A1, A2, B, and Injector C.

values clearly demonstrate that the spray plumes exhibit varying degrees of accuracy, highlighting their non-uniform behaviour.

Injector A1 exhibited variations in RMSE values across its plumes, indicating some variability in spray behaviour. These analyses suggest that A1's spray behaviour can vary under different conditions. In contrast, Injector-A2 (see Fig. 5.8(b)) consistently exhibited low RMSE values (around or below 2) for all its plumes (1 to 9), indicating reliable and symmetric spray behaviour. Similarly, Injector-B (see Fig.5.8(c)) displayed a behaviour similar to A2, with RMSE values consistently below 2 across its plumes, reinforcing its capability for producing symmetric spray patterns. On the other hand, Injector-C (see Fig. 5.8(d)) presented a more complex scenario, with most plumes having RMSE values below 2 but some showing notably higher values, signifying variations in spray penetration length. Unlike A2 and B, Injector C displayed less uniform RMSE values among its plumes, indicating a propensity for asymmetric spray behaviour and occasional fluctuations, possibly due to injector performance inconsistencies.

5.3 Summary of Spray Analysis Results at Increased Temperatures

5.3.1 Non-evaporative and non-reactive sprays

In evaporating sprays, fuel extends in vapour form beyond the liquid length. Penetration and cone angle are vital for spray research crucial for designing fuel injection system for internal combustion engines as they affect air-fuel mixing and combustion. Various factors like in-cylinder gas density, temperature, and injection pressure impact these parameters. This section further explores the influence of ambient density, fuel pressure and temperature on vapour penetration and cone angle under non-reactive at elevated temperature and pressure conditions.

5.3.2 Vapor penetration

The results in Figs.5.9(a) and 5.9(b) exhibit vapour penetration length versus time after fuel injection initiation. These figures offer insights into the effects of temperature and fuel pressure on vapour penetration at distinct ambient densities of 14.38 kg/m^3 or 27.24 kg/m^3, respectively. Figs.5.9(a) and 5.9(b) illustrate vapour penetration length over time under different conditions of fuel pressures and ambient temperatures. Distinct line patterns differentiate between the 2100 bar and 1700 bar fuel pressures. Continuous lines indicate a fuel pressure of 2100 bar, while dotted lines represent the 1700 bar condition. Legend colours provide a visual guide to the temperature conditions during each measurement. This detailed representation facilitates a deeper understanding of the intricate interaction between temperature, ambient density, and fuel pressure in shaping vapour penetration behavior.

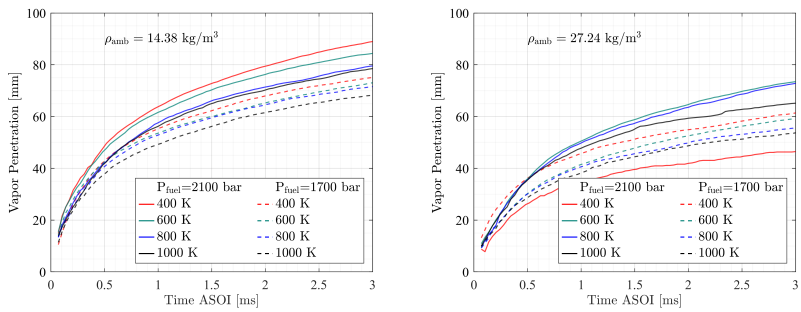

(a) (b)

Figure 5.9: A Comparative visualization of vapour penetration length over time under varied ambient densities and fuel pressures.

A notable observation can be noticed the inverse relationship between vapour

penetration length and ambient density. Vapour penetration length diminishes with an increase in ambient density, a trend that is clearly visible when contrasting the behaviours illustrated in the two figures. Figs.5.9(a), associated with the lower ambient density (14.38 kg/m^3), shows an extended penetration length compared to 5.9(b), which is characterized by a higher ambient density (27.24 kg/m^3). Furthermore, an analysis of the continuous and dotted lines within each figure reveals a direct correlation between vapour penetration length and fuel pressure. Vapour penetration increases significantly with an increase in fuel pressure from 1700 bar to 2100 bar. This behaviour is consistent trend across varying ambient densities. Moreover, an interesting trend arises when we look at how the temperature of the surrounding environment affects the length of vapor penetration. When the ambient temperature increases, the vapor penetration length decreases, as illustrated in the difference between 400 K and 1000 K in Figs.5.9(a) and 5.9(b).

5.3.3 Cone angle

Similarly, the cone angle exhibits a distinct relationship with ambient density. Notably, there are two key distinctions to highlight. Firstly, at lower ambient densities (14.38 kg/m^3), an increase in fuel pressure leads to an expansion of cone angles. However, at higher ambient densities (27.24 kg/m^3), an increase in fuel pressure causes a reduction in cone angles. This reversal of trends is in the opposite direction to the patterns observed at lower ambient densities as shown in Figs.5.10(b) and 5.10(b).

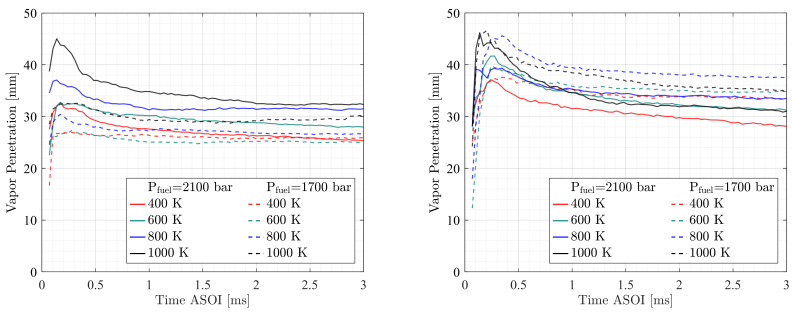

(a) Density= 14.38 kg/m^3 (b) Density= 27.24 kg/m^3

Figure 5.10: A Comparative visualization of cone angle over time under varied ambient densities and fuel pressures.

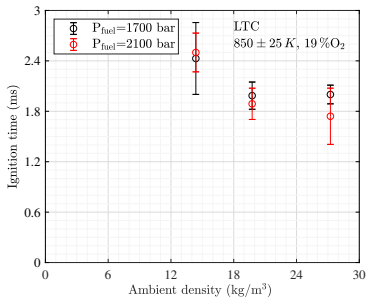

(a) Ignition time

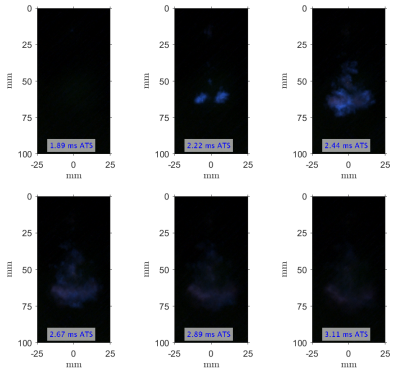

(b) Natural flame evolution at $\rho_{amb} = 14.38\,kg/m^3$,$P_{inj} = 210$ MPa

Figure 5.11: Depicting spray flames at 850 K

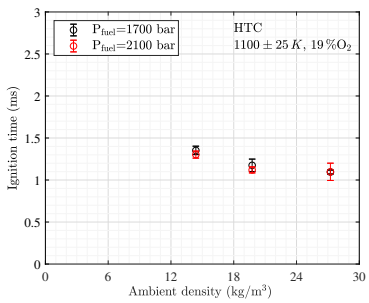

(a) Ignition time

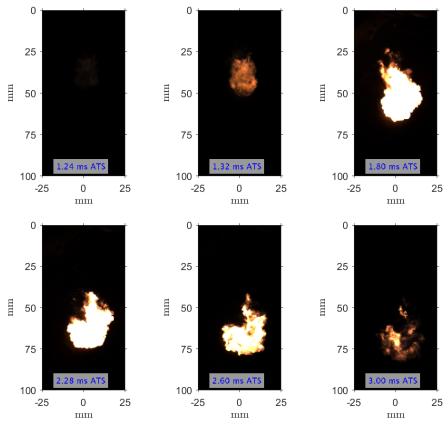

(b) Natural flame evolution at $\rho_{amb} = 14.38\,kg/m^3$,$P_{inj} = 210$ MPa

Figure 5.12: Depicting spray flames at 1150 K

5.3.4 Reactive sprays

5.3.5 Ignition time

In the hot phase experiments, reactive spray images were carefully captured and analyzed to explore the intricate dynamics of ignition time and spray flames. Various parameters influence these dynamics, including temperature,

fuel pressure, and ambient density. The images, systematically recorded at two pivotal temperature intervals—approximately 850 K and 1150 K—revealed complex patterns associated with the ignition and propagation of reactive sprays. A distinct pattern emerged at the 850 K threshold: ignition time inversely correlated with ambient density. An increase in ambient density precipitated a decrease in ignition time. This trend was captured in the reactive spray images, where spray flames, marked by a distinct blue colour (Fig. 5.11(b)), were distinctly visible, as depicted in Fig. 5.11(a). With the transition to the elevated temperature regime of 1150 K, a reduction in ignition time was observed, more pronounced than that at 850 K. This underscores the accelerated ignition processes occurring at higher temperatures and highlights the influential role of temperature on the reactivity and combustion kinetics of the sprays. Despite these temperature- and density-driven effects, fuel pressure shows no apparent influence on ignition time. This was illustrated in Figs. 5.11(b) and 5.12(b), where ignition time was non-responsive to variations in fuel pressure. This observation underscores the complexity of the factors that govern reactive sprays' ignition and combustion processes, with fuel pressure seemingly absent from this intricate process.

Chapter 6

Conclusions

The combined findings from these investigations offer valuable insights into the behaviour of multi-hole injectors and their effects on spray characteristics. It was noted that using the plume-blocking method resulted in increased spray penetration compared to other plume configurations. However, due to its rapid penetration, this approach may not be the most suitable choice for single-spray analyses. Moreover, it was observed that the plume-blocking technique alters the flow distribution within the sac volume, impacting spray properties significantly. Variations in spray patterns, especially during the initial injection stages, were attributed to manufacturing tolerances and needle oscillations, which tend to diminish over time. Overall, while the plume-blocking approach offers advantages in penetration, its applicability to single spray analysis may be limited. Conversely, a comprehensive examination of multi-hole injectors revealed substantial disparities in spray penetration length among individual plumes. This analysis encompassed average penetration values and the penetration lengths of individual plumes, highlighting significant deviations among plumes and underscoring the injector's inherent variability. Additionally, a comparative evaluation contrasted spray penetration length with that of corresponding thimble-generated sprays, emphasizing the reliability and precision of the thimble method for the study of single individual sprays, particularly in situations requiring precise control over spray behaviour. Notably, unique behaviours were identified among different injectors, with notable differences in spray penetration lengths in certain instances. However, a strong alignment was identified between thimble-generated sprays and those produced by multi-plume injectors, emphasizing the thimble method's reliability for single spray analysis. These studies also draw attention to the potential impact of manufacturing variations in injector nozzles on injector performance, highlighting the need for consideration in future enhancements of fuel injection processes.

Chapter 7

Future Work

7.1 Work Done So Far

The research has been centered on unravelling the intricate dynamics of sprays through a comprehensive investigation of various operational modes and their corresponding optical techniques, as outlined in Table. 3.1. A research project consists of four primary phases.

Phase-I: Non-reactive & Non-evaporative

In this initial phase, experiments were conducted using multi-plume configurations and Mie-scattering imaging methods. Additionally, the complexities of single-plume configurations, including plume-blocking and plume-thimble setups, alongside the utilization of diffuse back-light imaging, were explored. These completed experiments constitute a significant portion of the research findings. Specifically, four injectors were tested: A1, A2, B, and C, both with a thimble (plume-thimble) and without (multi-plume). The two papers are currently under review based on the results of Phase-I.

Phase-II: Non-reactive & Evaporative

In the subsequent phase, the focus shifted to experiments primarily centred around single-plume configurations using a specific injector, namely Injector-B. Notably, emphasis was placed on the thimble configuration. Various optical methods were employed, including diffuse back-light, shadowgraph, and Schlieren techniques. All experiments within this phase have been successfully concluded, providing valuable insights into the behaviour of evaporating sprays.

Phase-III: Reactive Sprays

The research journey progressed into reactive sprays, where single-plume thimble configurations with the same injector, B, were utilized. Optical techniques such as shadowgraphy, Schlieren, and luminosity measurements were employed. The experiments in this phase are complete, and active engagement is underway in the analysis phase, where the data is being prepared for peer review and publication.

7.2 Current Status

The research is in the final stages of data analysis and paper writing for the experiments conducted in Phase-II and Phase-III. This involves a comprehensive analysis of shadowgraphy, Schlieren, and luminosity data, all of which play a pivotal role in comprehending the intricacies of both non-reactive and evaporative and reactive spray behaviour. Diligent efforts are being made to ensure the research findings are meticulously documented and poised for submission to academic journals. Looking ahead, the immediate priority is to finalize the two research papers from the experiments conducted during the non-reactive, evaporative, and reactive spray phases and submit them for peer review.

Phase-IV: Ballistic Imaging:

Simultaneously, there is active involvement in an ongoing experiment that involves implementing ballistic imaging techniques. This endeavour aims to provide deeper insights into the dynamics of sprays in the near-field region, further enriching the research.

Chapter 8

Contributions

Paper-I

"*Shape/penetration analysis of isolated spray plumes in a multi-hole Diesel spray*"

The main author conducted this research project in collaboration with co-authors. The study examined the spray morphology of a multi-hole diesel fuel injector within a constant-volume spray chamber, employing two different methodologies for plume isolation. One method used a thimble-equipped nozzle to isolate single plumes, while the other involved plume-blocking by sealing the nozzle's orifices. The findings revealed that the plume-blocking approach resulted in greater penetration depth than the thimble-equipped nozzle. However, this method is better suited for single-spray studies due to its rapid penetration. Distinct spray disparities were also observed from a clogged nozzle compared to an unblocked one, while the thimble-equipped nozzle exhibited behaviour similar to a standard nozzle. These observations show how sealed orifices modify flow distribution within the sac volume, subsequently affecting spray characteristics. In summary, the research was collaborative, with the main author primarily responsible for experimental design, meticulous data collection, analysis, and manuscript preparation. This study enhances the understanding of plume isolation techniques and their impact on spray morphology, providing valuable insights into spray behaviour under varying conditions.

Paper-II

"*Manufacturing disparities and their effect on transient spray characteristics in Diesel injectors*"

This study, a collaborative effort with the main author's co-authors, addresses concerns regarding inconsistent diesel injector performance attributed

to manufacturing variations. We systematically analysed sprays from four different diesel injectors with multi-hole nozzles, focusing on their characteristics under diverse injection conditions. Variations in hole dimensions were identified as significant factors affecting spray and mixing processes. Experiments were conducted in an optically accessible combustion vessel under various conditions, providing insights into spray behaviour. We employed a Root Mean Square Error (RMSE) methodology to analyse spray penetration length variations among the injectors, uncovering symmetric and asymmetric spray behaviours. The main author conducted experiments, analysed data, and prepared the manuscript with co-author contributions. This research enhances understanding of diesel injector performance and addresses challenges related to manufacturing variations.

Bibliography

[1] S Okajima and S Kumagai, "Experimental investigation of soot and nox reduction by impinging spray combustion in a closed vessel," *Symposium (International) on Combustion*, vol. 23, pp. 275–279, 1 Jan. 1991, ISSN: 00820784. DOI: 10.1016/S0082-0784(06)80270-5. [Online]. Available: https://linkinghub.elsevier.com/retrieve/pii/S0082078406802705 (cit. on p. 3).

[2] A. K. Agarwal, T. Gupta, P. C. Shukla and A. Dhar, "Particulate emissions from biodiesel fuelled ci engines," *Energy Conversion and Management*, vol. 94, pp. 311–330, Apr. 2015, ISSN: 01968904. DOI: 10.1016/j.enconman.2014.12.094. [Online]. Available: https://linkinghub.elsevier.com/retrieve/pii/S0196890415000023 (cit. on p. 3).

[3] K. K. Srinivasan, S. R. Krishnan and Y Qi, "Cyclic combustion variations in dual fuel partially premixed pilot-ignited natural gas engines," *Journal of Energy Resources Technology*, vol. 136, p. 12 003, 1 Mar. 2014, ISSN: 0195-0738, 1528-8994. DOI: 10.1115/1.4024855. [Online]. Available: https://asmedigitalcollection.asme.org/energyresources/article/doi/10.1115/1.4024855/366565/Cyclic-Combustion-Variations-in-Dual-Fuel (cit. on p. 3).

[4] L. Wei and P. Geng, "A review on natural gas/diesel dual fuel combustion, emissions and performance," *Fuel Processing Technology*, vol. 142, pp. 264–278, 2016 (cit. on p. 3).

[5] S. Kumar, H. T. Kwon, K. H. Choi *et al.*, "Lng: An eco-friendly cryogenic fuel for sustainable development," *Applied Energy*, vol. 88, pp. 4264–4273, 12 Dec. 2011, ISSN: 0306-2619. DOI: 10.1016/J.APENERGY.2011.06.035 (cit. on p. 3).

[6] R Chandra, V. K. Vijay, P. M. V. Subbarao and T. K. Khura, "Performance evaluation of a constant speed ic engine on cng, methane enriched biogas and biogas," *Applied Energy*, vol. 88, pp. 3969–3977, 11 Nov. 2011, ISSN: 03062619. DOI: 10.1016/j.apenergy.2011.04.032. [Online]. Available: https://linkinghub.elsevier.com/retrieve/pii/S0306261911002546 (cit. on p. 3).

[7] P. Sombatwong, P. Thaiyasuit and K. Pianthong, "Effect of pilot fuel quantity on the performance and emission of a dual producer gas–diesel engine," *Energy Procedia*, vol. 34, pp. 218–227, 2013, ISSN: 18766102. DOI: 10.1016/j.egypro.2013.06.750. [Online]. Available: https://linkinghub.elsevier.com/retrieve/pii/S1876610213009934 (cit. on p. 3).

[8] C. C. Pounder and D. F. Woodyard, *Pounder's marine diesel engines and gas turbines*, 8th ed. Elsevier Butterworth Heinemann, 2004, OCLC: ocm53231381, ISBN: 978-0-7506-5846-1 (cit. on p. 3).

[9] R. S. Baert, P. J. Frijters, B. Somers, C. C. Luijten and W. D. Boer, "Design and operation of a high pressure, high temperature cell for hd diesel spray diagnostics: Guidelines and results," 2009. DOI: 10.4271/2009-01-0649 (cit. on pp. 4, 10, 22).

[10] L. M. Pickett, C. L. Genzale, G. Bruneaux *et al.*, "Comparison of diesel spray combustion in different high-temperature, high-pressure facilities," *SAE Int. J. Engines*, vol. 3, p. 27, 2 2022 (cit. on p. 4).

[11] F. Payri, R. Payri, M. Bardi and M. Carreres, "Engine combustion network: Influence of the gas properties on the spray penetration and spreading angle," *Experimental Thermal and Fluid Science*, vol. 53, pp. 236–243, Feb. 2014, ISSN: 0894-1777. DOI: 10.1016/J.EXPTHERMFLUSCI.2013.12.014 (cit. on p. 4).

[12] D. Deshmukh, "Studies on atomization and sprays of plant oil biofuels using laser-based diagnostics," Ph.D. Thesis, Indian Institute of Science, Bangalore, 2011 (cit. on pp. 4, 10).

[13] M. K. Pal and S. Bakshi, "Study of the effect of ambient vapour concentration on the spray structure of an evaporating n-hexane spray," *Experimental Thermal and Fluid Science*, vol. 88, pp. 566–575, Nov. 2017, ISSN: 0894-1777. DOI: 10.1016/J.EXPTHERMFLUSCI.2017.07.013 (cit. on p. 4).

[14] Y. Jin, J. Kim, S. Kakami, K. Nishida, Y. Ogata and H. Luo, "Comparison of diesel spray with small injection amount between single-hole and multi-hole injectors: Results under same rail pressure and similar injection rate," *International Communications in Heat and Mass Transfer*, vol. 118, 2020, ISSN: 07351933. DOI: 10.1016/j.icheatmasstransfer.2020.104862 (cit. on p. 4).

[15] Z. He, W. Zhong, Q. Wang, Z. Jiang and Z. Shao, "Effect of nozzle geometrical and dynamic factors on cavitating and turbulent flow in a diesel multi-hole injector nozzle," *International Journal of Thermal Sciences*, vol. 70, pp. 132–143, Aug. 2013, ISSN: 1290-0729. DOI: 10.1016/J.IJTHERMALSCI.2013.03.008 (cit. on p. 4).

[16] R. J. Klein-Douwel, P. J. Frijters, L. M. Somers, W. A. de Boer and R. S. Baert, "Macroscopic diesel fuel spray shadowgraphy using high speed digital imaging in a high pressure cell," *Fuel*, vol. 86, 12-13 2007, ISSN: 00162361. DOI: 10.1016/j.fuel.2006.11.039 (cit. on p. 4).

[17] J. Naber and D. L. Siebers, "Effects of gas density and vaporization on penetration and dispersion of diesel sprays," Feb. 1996, p. 960 034. DOI: 10.4271/960034. [Online]. Available: https://www.sae.org/content/960034/ (cit. on pp. 4, 19).

[18] W. E. Eagle, S. B. Morris and M. S. Wooldridge, "High-speed imaging of transient diesel spray behavior during high pressure injection of a multi-hole fuel injector," *Fuel*, vol. 116, pp. 299–309, Jan. 2014, ISSN: 00162361. DOI: 10.1016/j.fuel.2013.07.120 (cit. on p. 4).

[19] R. Payri, J. P. Viera, V. Gopalakrishnan and P. G. Szymkowicz, "The effect of nozzle geometry over internal flow and spray formation for three different fuels," *Fuel*, vol. 183, pp. 20–33, 2016, ISSN: 0016-2361. DOI: https://doi.org/10.1016/j.fuel.2016.06.041. [Online]. Available: https://www.sciencedirect.com/science/article/pii/S0016236116304938 (cit. on p. 4).

[20] M. Bardi, R. Payri, L. M. C. Malbec *et al.*, "Engine combustion network: Comparison of spray development, vaporization, and combustion in different combustion vessels," *Atomization and Sprays*, vol. 22, no. 10, 2012 (cit. on pp. 4, 9, 10).

[21] D. Kennaird, C. Crua, J. Lacoste, M. Heikal, M. Gold and N. Jackson, "In-cylinder penetration and break-up of diesel sprays using a common-rail injection system," SAE Technical Paper, Tech. Rep., 2002 (cit. on p. 5).

[22] C. He, Y. Ge, J. Tan and X. Han, "Spray properties of alternative fuels: A comparative analysis of biodiesel and diesel," *International journal of energy research*, vol. 32, no. 14, pp. 1329–1338, 2008 (cit. on p. 5).

[23] H. Xie, L. Song, Y. Xie, D. Pi, C. Shao and Q. Lin, "An experimental study on the macroscopic spray characteristics of biodiesel and diesel in a constant volume chamber," *Energies*, vol. 8, no. 6, pp. 5952–5972, 2015, ISSN: 1996-1073. DOI: 10.3390/en8065952. [Online]. Available: https://www.mdpi.com/1996-1073/8/6/5952 (cit. on pp. 5, 17).

[24] C. Espey and J. E. Dec, "Diesel engine combustion studies in a newly designed optical-access engine using high-speed visualization and 2-d laser imaging," in *International Congress & Exposition*, SAE International, 1993. DOI: https://doi.org/10.4271/930971. [Online]. Available: https://doi.org/10.4271/930971 (cit. on p. 9).

[25] M. Mittal, D. L. Hung, G. Zhu and H. J. Schock, "Fuel spray visualization and its impingement analysis on in-cylinder surfaces in a direct-injection spark-ignition engine," *Journal of visualization*, vol. 14, pp. 149–160, 2011 (cit. on p. 9).

[26] T. Kamimoto, H. Kando, S. Kobori, H. Hatano, H. Kobayashi and K. Tsuchiya, "Development of a rapid compression-expansion machine to simulate combustion in diesel engines," in *1988 SAE International Fall Fuels and Lubricants Meeting and Exhibition*, SAE International, 1988. DOI: https://doi.org/10.4271/881640. [Online]. Available: https://doi.org/10.4271/881640 (cit. on p. 9).

[27] W. Du, J. Lou, Y. Yan, W. Bao and F. Liu, "Effects of injection pressure on diesel sprays in constant injection mass condition," *Applied Thermal Engineering*, vol. 121, pp. 234–241, 2017 (cit. on p. 10).

[28] N. Otsu, "A threshold selection method from gray-level histograms," *IEEE Transactions on Systems, Man, and Cybernetics*, vol. 9, no. 1, pp. 62–66, 1979. DOI: 10.1109/TSMC.1979.4310076 (cit. on pp. 16, 17, 24).

[29] J. V. Pastor, J. Arrègle, J. M. García and L. D. Zapata, "Segmentation of diesel spray images with log-likelihood ratio test algorithm for non-gaussian distributions," *Applied Optics*, vol. 46, p. 888, 6 Feb. 2007, ISSN: 0003-6935, 1539-4522. DOI: 10.1364/AO.46.000888. [Online]. Available: https://opg.optica.org/abstract.cfm?URI=ao-46-6-888 (cit. on p. 16).

[30] V Macian, R Payri, A Garcia and M Bardi, "Experimental evaluation of the best approach for diesel spray images segmentation," *Experimental Techniques*, vol. 36, pp. 26–34, 6 Nov. 2012, ISSN: 07328818. DOI: 10.1111/j.1747-1567.2011.00730.x. [Online]. Available: http://doi.wiley.com/10.1111/j.1747-1567.2011.00730.x (cit. on p. 16).

[31] R. Payri, J. Gimeno, J. P. Viera and A. H. Plazas, "Needle lift profile influence on the vapor phase penetration for a prototype diesel direct acting piezoelectric injector," *Fuel*, vol. 113, pp. 257–265, Nov. 2013, ISSN: 00162361. DOI: 10.1016/j.fuel.2013.05.057. [Online]. Available: https://linkinghub.elsevier.com/retrieve/pii/S0016236113004699 (cit. on p. 16).

[32] J Shao, Y Yan, G Greeves and S Smith, "Quantitative characterization of diesel sprays using digital imaging techniques," *Measurement Science and Technology*, vol. 14, pp. 1110–1116, 7 Jul. 2003, ISSN: 0957-0233, 1361-6501. DOI: 10.1088/0957-0233/14/7/328. [Online]. Available: https://iopscience.iop.org/article/10.1088/0957-0233/14/7/328 (cit. on pp. 17, 19).

[33] E Delacourt, B Desmet and B Besson, "Characterisation of very high pressure diesel sprays using digital imaging techniques," *Fuel*, vol. 84, pp. 859–867, 7-8 May 2005, ISSN: 00162361. DOI: 10.1016/j.fuel.2004.12.003. [Online]. Available: https://linkinghub.elsevier.com/retrieve/pii/S0016236105000062 (cit. on pp. 17, 19).

[34] G. Rubio-Gómez, S Martínez-Martínez, L. F. Rua-Mojica, P. Gómez-Gordo and O. A. de la Garza, "Automatic macroscopic characterization of diesel sprays by means of a new image processing algorithm," *Measurement Science and Technology*, vol. 29, p. 55 406, 5 May 2018, ISSN: 0957-0233, 1361-6501. DOI: 10.1088/1361-6501/aab121. [Online]. Available: https://iopscience.iop.org/article/10.1088/1361-6501/aab121 (cit. on p. 17).

[35] R. Payri, J. Gimeno, G. Bracho and D. Vaquerizo, "Study of liquid and vapor phase behavior on diesel sprays for heavy duty engine nozzles," *Applied Thermal Engineering*, vol. 107, 2016, ISSN: 13594311. DOI: 10.1016/j.applthermaleng.2016.06.159 (cit. on p. 17).

[36] M. K. Pal and S. Bakshi, "Effect of ambient fuel vapour concentration on the vapour penetration of evaporating n-hexane sprays," *Fuel*, vol. 223, pp. 179–187, Jul. 2018, ISSN: 00162361. DOI: 10.1016/j.fuel.2018.02.193. [Online]. Available: https://linkinghub.elsevier.com/retrieve/pii/S0016236118303892 (cit. on p. 17).

[37] R Payri, F. J. Salvador, J Gimeno and J de la Morena, "Macroscopic behavior of diesel sprays in the near-nozzle field," *SAE International Journal of Engines*, vol. 1, pp. 528–536, 1 Apr. 2008, ISSN: 1946-3944. DOI: 10.4271/2008-01-0929. [Online]. Available: https://www.sae.org/content/2008-01-0929/ (cit. on p. 19).

[38] G. Rubio-Gómez, S Martínez-Martínez, L. F. Rua-Mojica, P. Gómez-Gordo and O. A. de la Garza, "Automatic macroscopic characterization of diesel sprays by means of a new image processing algorithm," *Measurement Science and Technology*, vol. 29, p. 55 406, 5 May 2018, ISSN: 0957-0233, 1361-6501. DOI: 10.1088/1361-6501/aab121. [Online]. Available: https://iopscience.iop.org/article/10.1088/1361-6501/aab121 (cit. on p. 19).

[39] F Payri, R. Payri, M. Bardi and M Carreres, "Engine combustion network: Influence of the gas properties on the spray penetration and spreading angle," *Experimental Thermal and Fluid Science*, vol. 53, pp. 236–243, 2014 (cit. on p. 19).

[40] D. R. Emberson, B Ihracska, S Imran and A Diez, "Optical characterization of diesel and water emulsion fuel injection sprays using shadowgraphy," *Fuel*, vol. 172, pp. 253–262, May 2016, ISSN: 00162361. DOI: 10.1016/j.fuel.2016.01.015. [Online]. Available: https://linkinghub.elsevier.com/retrieve/pii/S0016236116000247 (cit. on p. 19).

[41] C. K. Suraj, G Sudarshan, K Anand and T Sundararajan, "Effects of autooxidation on the fuel spray characteristics of karanja biodiesel," *Biomass and Bioenergy*, vol. 149, p. 106 084, Jun. 2021, ISSN: 09619534. DOI: 10.1016/j.biombioe.2021.106084. [Online]. Available: https://linkinghub.elsevier.com/retrieve/pii/S0961953421001215 (cit. on p. 19).

[42] P. V. Farrell, C. T. Chang and T. F. Su, "High pressure multiple injection spray characteristics," Feb. 1996, p. 960 860. DOI: 10.4271/960860. [Online]. Available: https://www.sae.org/content/960860/ (cit. on p. 19).

[43] P. Dong, K. Nishida, T. Inaba and Y. Ogata, "Characterization of internal flow and spray behaviors of hole-type nozzle under tiny and normal injection quantity conditions for diesel engine," *SAE International Journal of Fuels and Lubricants*, vol. 9, pp. 125–137, 1 Apr. 2016, ISSN:

1946-3960. DOI: 10.4271/2016-01-0862. [Online]. Available: https://www.sae.org/content/2016-01-0862/ (cit. on p. 19).

[44] R. Payri, J. Gimeno, G. Bracho and D. Vaquerizo, "Study of liquid and vapor phase behavior on diesel sprays for heavy duty engine nozzles," *Applied Thermal Engineering*, vol. 107, 2016, ISSN: 13594311. DOI: 10.1016/j.applthermaleng.2016.06.159 (cit. on p. 19).

[45] I. Ruiz-Rodriguez, R. Pos, T. Megaritis and L. C. Ganippa, "Investigation of spray angle measurement techniques," *IEEE Access*, vol. 7, pp. 22 276–22 289, 2019, ISSN: 2169-3536. DOI: 10.1109/ACCESS.2019.2899214. [Online]. Available: https://ieeexplore.ieee.org/document/8641265/ (cit. on p. 19).

[46] G. S. Settles, *Schlieren and shadowgraph techniques: visualizing phenomena in transparent media*. Springer Science & Business Media, 2001 (cit. on p. 24).

[47] L. M. Pickett, S. Kook and T. C. Williams, "Visualization of diesel spray penetration, cool-flame, ignition, high-temperature combustion, and soot formation using high-speed imaging," *SAE international journal of engines*, vol. 2, no. 1, pp. 439–459, 2009 (cit. on p. 24).

[48] Y. Ma, S. Huang, R. Huang, Y. Zhang and S. Xu, "Spray and evaporation characteristics of n-pentanol–diesel blends in a constant volume chamber," *Energy Conversion and Management*, vol. 130, pp. 240–251, 2016 (cit. on p. 24).

[49] F. Luo, H. Cui and S. Dong, "Transient measuring method for injection rate of each nozzle hole based on spray momentum flux," *Fuel*, vol. 125, pp. 20–29, Jun. 2014, ISSN: 00162361. DOI: 10.1016/j.fuel.2014.02.011. [Online]. Available: https://linkinghub.elsevier.com/retrieve/pii/S0016236114001446 (cit. on p. 30).

[50] M. K. Pal and A. Bhagwat, "Comparison of a single-plume-spray with a multi-plume-spray from a multi-hole common-rail diesel injector," *ICLASS 2015, Tainan, Taiwan, August 23–27*, p. 8, 2015 (cit. on p. 30).

[51] M. Battistoni, Q. Xue, S. Som and E. Pomraning, "Effect of off-axis needle motion on internal nozzle and near exit flow in a multi-hole diesel injector," *SAE International Journal of Fuels and Lubricants*, vol. 7, pp. 167–182, 1 Apr. 2014, ISSN: 1946-3960. DOI: 10.4271/2014-01-1426. [Online]. Available: https://www.sae.org/content/2014-01-1426/ (cit. on p. 31).

[52] C. Wang, A. Moro, F. Xue, X. Wu and F. Luo, "The influence of eccentric needle movement on internal flow and injection characteristics of a multi-hole diesel nozzle," *International Journal of Heat and Mass Transfer*, vol. 117, pp. 818–834, Feb. 2018, ISSN: 00179310. DOI: 10.1016/j.ijheatmasstransfer.2017.10.057. [Online]. Available: https://linkinghub.elsevier.com/retrieve/pii/S0017931017325450 (cit. on p. 31).